

# Tectonics

## RESEARCH ARTICLE

10.1029/2020TC006491

### Key Points:

- An oblique shale-detachment fold laterally separates two sets of major fold-thrusts with synchronous evolution history
- The deformation process is determined by shale redistribution due to differential contraction and differential syntectonic sediment loading
- Seismic-observed deformations within the shale units include multiscale brittle failures, ductile folding, and local flow of shales

### Correspondence to:

J. Zhang and S. Wu,  
[zhangjiajia0103@outlook.com](mailto:zhangjiajia0103@outlook.com);  
[reser@cup.edu.cn](mailto:reser@cup.edu.cn)




### Citation:

Zhang, J., Wu, S., Hu, G., Yue, D., Xu, Z., Chen, C., et al. (2021). Role of shale deformation in the structural development of a deepwater gravitational system in the Niger Delta. *Tectonics*, 40, e2020TC006491. <https://doi.org/10.1029/2020TC006491>

Received 21 AUG 2020

Accepted 19 APR 2021

## Role of Shale Deformation in the Structural Development of a Deepwater Gravitational System in the Niger Delta

Jiajia Zhang<sup>1</sup> , Shenghe Wu<sup>1</sup> , Guangyi Hu<sup>2</sup>, Dali Yue<sup>1</sup> , Zhenhua Xu<sup>1</sup>, Cheng Chen<sup>2</sup>, Ke Zhang<sup>1</sup>, Junjie Wang<sup>1</sup>, and Siying Wen<sup>1</sup>

<sup>1</sup>College of Geosciences, State Key Laboratory of Petroleum Resource and Prospecting, China University of Petroleum (Beijing), Beijing, China, <sup>2</sup>Research Institute, China National Offshore Oil Corporation, Beijing, China

**Abstract** This paper presents a three-dimensional (3D) seismic-based case study (~1,200 km<sup>2</sup>) from the deepwater Niger Delta to examine the role of shale deformation in the structural development of a deepwater gravitational system. Tectono-stratigraphic interpretation reveals that this system consists of two sets of major fold-thrusts laterally separated by a central oblique detachment fold. A prominent shale thick beneath these structures is believed to have originated from tectonic deformation rather than a pre-tectonic thick, due to its complex internal structures. Seismic mapping of the growth units indicates synchronous initiation of the oblique detachment fold with the main thrusts and gradual growth in response to thickening shales. Downslope gravitational contraction is not considered the direct cause for the oblique shale-detachment fold. Evidence from the 3D shale distribution and deformation styles within the shale unit reveals that shales that were squeezed out of adjacent shale-thinning areas “flowed” laterally into the detachment-fold core. Based on the spatial variation in structural deformation and growth strata distribution, this study proposes a model that considers differential contraction and differential loading from syntectonic sediments as two key factors leading to the 3D shale redistribution which ultimately determines the deformation styles and evolution history within the overburden. Additionally, seismic imaging within the shale unit recognizes various internal structures ranging from hundreds to thousands of meters in scale, and confirms what has been suggested in previous studies, that redistribution of shales occurred through a combination of multiscale brittle failures, ductile folding, and plastic flows.

## 1. Introduction

Deepwater gravitational systems are characterized by gravity-driven thrusts and folds developed at the downdip end of passive margins, which may exert significant impacts on the deepwater sedimentary process (e.g., Clark & Cartwright, 2009, 2011, 2012; Gee & Gawthorpe, 2006; Huyghe et al., 2004; Jolly et al., 2016, 2017; Mayall et al., 2010; Oluboyo et al., 2014; Rowan et al., 2004). Contractional deformations driven by gravitational collapse of advancing deltaic sediment wedges are largely accommodated by thin-skinned thrusting and folding above a regionally extensive decollement of weak salt or shale units, which form the gravity-driven fold and thrust belts (e.g., Bilotti & Shaw, 2005; Cohen & McClay, 1996; Morley & Guerin, 1996; Rouby et al., 2011; Rowan et al., 2004; Wu & Bally, 2000). Currently, many studies have revealed the geometries, evolution histories, and kinematic models of gravity-driven fold and thrust belts (e.g., Bergen & Shaw, 2010; Corredor et al., 2005; Gao et al., 2018; Higgins et al., 2007; Jolly et al., 2016; King & Morley, 2017; Mahanjane & Franke, 2014; Maloney et al., 2010; Morley et al., 2011, 2017; Nyantakyi et al., 2015; Sun & Liu, 2018; Totake et al., 2018; Yang et al., 2020).

The Niger Delta basin is one of the classic shale tectonic province in the world where deepwater gravitational systems are widely developed and studied (e.g., Cohen & McClay, 1996; Corredor et al., 2005; Damuth, 1994; Jolly et al., 2017, 2016; Morley & Guerin, 1996; Pizzi et al., 2020; Rouby et al., 2011; Wu & Bally, 2000; Wu et al., 2015). Previous studies found that the structural development of deepwater gravitational systems is closely related to deformation within the ductile substrate, composed of undercompacted and overpressured mobile shales (e.g., Bonini, 2003; Cohen & McClay, 1996; Deville et al., 2006; Duerto & McClay, 2011; Fillon et al., 2013; Hansberry et al., 2014; Morley, 2003; Morley & Guerin, 1996; Morley et al., 2011, 2017, 1998; Wu & Bally, 2000). Shale deformations change shale thickness (either thickening or thinning) and are associated with horizontal slips above single or multiple detachment surfaces.

Fault kinematic studies on typical fault-propagation, fault-bend, and detachment folds (Jamison, 1987; Mitra, 1990; Suppe, 1983) suggest that deformation within the basal shale unit occurs synchronously with deformation operating within the overburden, and the thick mobile detachments can facilitate additional deformation styles and modifiers. An updated model of break-thrust style folds suggests local shale thickening triggered by structural shortening can precede development of large break thrusts, and these break thrusts subsequently propagate downward to join the basal detachment rather than propagate upward from a master detachment (e.g., Morley, 2009; Morley & Naghadeh, 2018; Morley et al., 2017). In the southern lobe of the deepwater Niger Delta, Maloney et al. (2010) identified an entirely separate postfaulting thickness change within the basal shale unit that led to continual uplift following the early phase thrust-propagation folding. These studies show great variability of shale deformation which leads to different evolution histories in the sedimentary overburden.

Despite growing interest in shale-related structures, the 3D deformation process of the basal shale unit and how shale deformations interact with the evolution of deformation styles in the overburden remain poorly understood. Previous fault kinematic models typically assume that contractional shortening in both the basal shale unit and the overburden occurs primarily downslope due to gravitational collapse above detachment surface (e.g., Briggs et al., 2006; Corredor et al., 2005; Morley, 2009; Maloney et al., 2010, 2017; Suppe, 1983). The resulting thrusts and folds strike essentially perpendicular to the regional slope. Besides regional gravity-driven contraction, local variation in the pore-fluid pressure also has a role in facilitating shale deformation and the basal shale units can be squeezed from areas of high pore-fluid pressure to areas of lower pore-fluid pressure (e.g., Morley et al., 2017). If local squeezing of shales occurs along the strike of a continental slope, it may yield structures striking oblique or perpendicular to the strike of the main structures. Incorporating the effect of local shale squeezing into classic fault kinematic models would enable a better understanding of the 3D deformation process of the basal shale unit. Within the sedimentary overburden, the sedimentary growth sequences deposited coevally with deformation have varying geometries and strain rates that record the structural evolution history (e.g., Burbank & Verges, 1994; Burbank et al., 1996; Jolly et al., 2016, 2017; Morley & Leong, 2008; Pizzi et al., 2020; Poblet et al., 1997; Suppe et al., 1992). Evidence of a correlation between 3D shale deformation and growth sequence evolution is still rare in existing literature. Therefore, the main objective of this study is to better understand the interaction between shale deformation and growth of thrusts and folds in the overburden.

Seismic reflection data are a useful tool to study the deformational structures within deeply buried shales, though seismic-observed deformations can be larger scale than the deformations observed on outcrops or wells. As seismic resolution is limited, controversy regarding deformation mechanisms (ductile vs. brittle deformations) within a basal shale unit remains. Brittle deformation is a result of brittle failures in the shales while ductile deformation refers to ductile movement due to a partial or complete loss of shear strength. Early work on the Niger Delta identified the existence of mobile shales or shale diapirs (e.g., Ajakaiye & Bally, 2002; Cohen & McClay, 1996; Damuth, 1994; Krueger & Grant, 2011; Morley & Guerin, 1996; Wiener et al., 2010; Wu & Bally, 2000), which were assumed to have deformed analogous to mobile salt units in other systems that flow plastically in response to sediment loading (e.g., Brun & Fort, 2004; Curry et al., 2018; Giles & Rowan, 2012; Hudec et al., 2009; Jackson & Talbot, 1986; Kergaravat et al., 2016; Kopriva & Kim, 2015; Schleder et al., 2019; Sylvester et al., 2015). With higher-quality seismic data acquired subsequently, studies revealed many transparent reflections previously observed within the shale units are actually incoherent reflections, resulting in the reinterpretation of shale tectonic features as second-order folds or thrusts with dominant brittle deformation in the shales (e.g., Couzens-Schultz et al., 2003; Maloney et al., 2010; Morgan, 2015; Morley et al., 2011, 2017; Plesch et al., 2007). Consequently, there are far fewer examples of bona fide shale tectonic features where ductile shale has withdrawn and provided space to trap sediment. Some recent studies argue that mobile shales and shale-withdrawal minibasins do at times exist (e.g., Blanchard et al., 2019; Dean et al., 2015; Duerto & McClay, 2011; Galindo & Lonergan, 2020; Ings & Beaumont, 2010; Ruh et al., 2018; Soto et al., 2010). The combination of brittle and ductile shale deformations may be significant for effective accommodation of the shortening deformation in the overburden (Duerto & McClay, 2011; Maloney et al., 2010; Morley et al., 2011, 2017, 2018; Van Rensbergen & Morley, 2003). The debate on deformation mechanisms within the shale-prone units suggests considerable case-by-case variation in shale deformation. Additional research, especially with the use of high-quality 3D

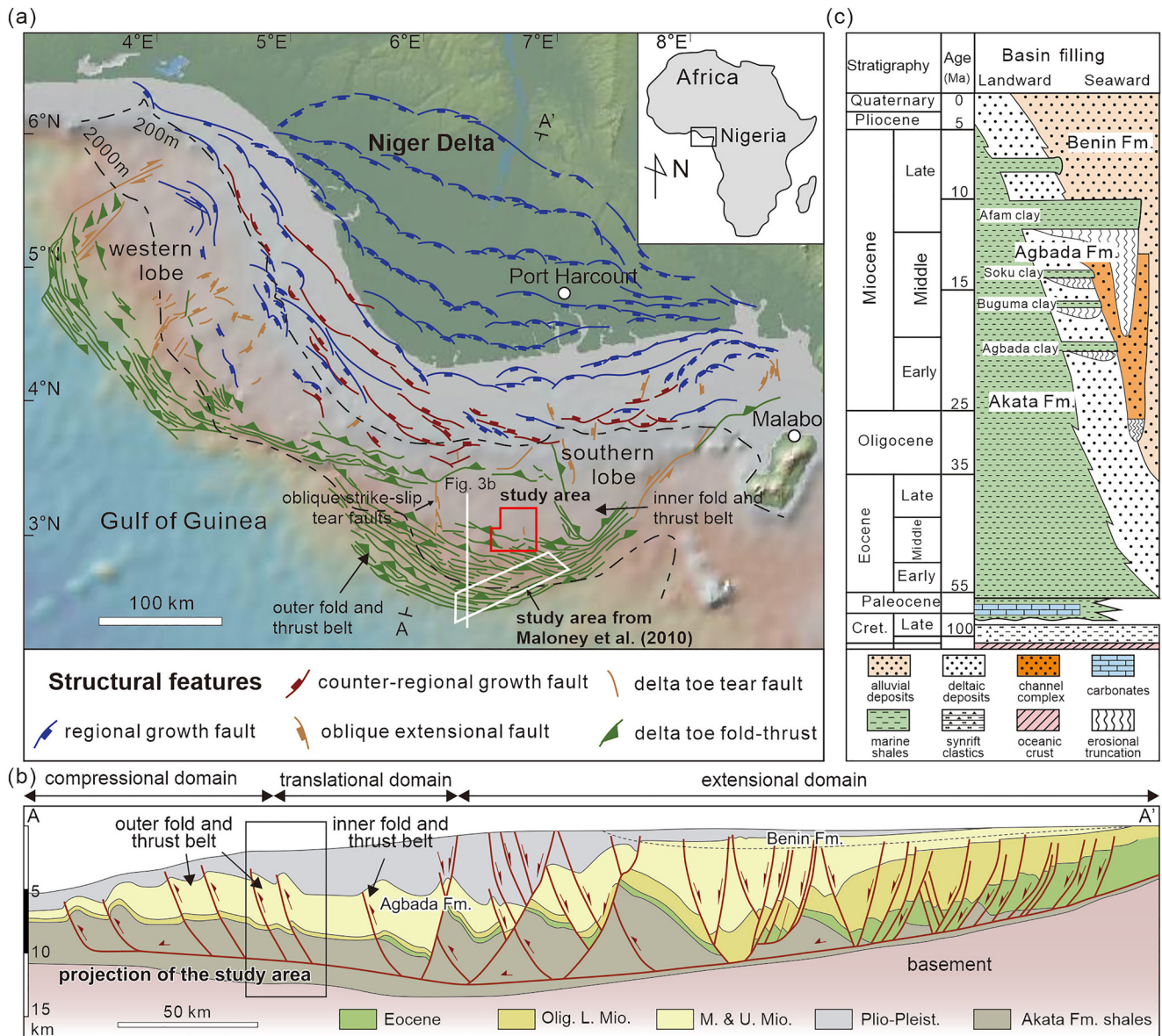


**Figure 1.** Regional structure map (a) and cross section (b) of the Niger Delta showing the distribution of gravity-driven structural domains across the basin, after Wu et al. (2015). The study area is located at a site between the translational and compressional domain, north of the study area from Maloney et al. (2010). The brown colored lines on (a) represent a series of oblique extensional faults and strike-slip tear faults scattered among the main structures. (c) Regional stratigraphy of the Niger Delta showing three diachronous lithological units (Akata, Agbada, and Benin formations) prograding seaward since Eocene, after Corredor et al. (2005). The studied interval involves the late Oligocene-to-present Agbada clastic deposits and the Akata shales.

seismic reflection data, is needed to better understand the complexity and variability of deformation mechanisms occurring within deeply buried shale units.

This study focuses on a deepwater gravitational system in the Niger Delta, specifically located at a site between the outer fold and thrust belts and translational zone (Figure 1a). This system is underlain by thick, deformed shale units with notable thickness variations and complex internal structures. High-quality 3D seismic reflection data presents clear imaging of the thrust-related structures and mapping of growth units reveals the evolution of these structures. By detailing a correlation between shale deformation and structural growth history, this paper addresses two key questions on shale-related structures: (1) how the basal shale unit has deformed in space and how interactions with the overlying thrusting and folding has changed over time; (2) what kind of deformation mechanisms (brittle vs. ductile deformations) have occurred within the

basal shale unit that essentially resulted in shale movement and structural evolution. This study provides new insight into the role of shale deformation in the structural development of deepwater gravitational systems while complementing previous studies on geometrical-kinematic models of shale-related structures.

## 2. Geological Background

The Niger Delta basin is located in the Gulf of Guinea on the passive margin of western Africa (Figure 1a). The basin evolution went through an early rifting stage prior to the late Cretaceous which then transitioned into the late drifting stage until present day (Uchupi, 1989). As one of the largest deltas in the world (Doust & Omatsola, 1990), the Niger Delta has developed largely since the Eocene with large volumes of marine clastic materials deposited across the basin margin, forming a sedimentary prism of  $\sim 140,000$  km<sup>2</sup> in area and up to 12-km thick (Briggs et al., 2006; Cohen & McClay, 1996). In the shelf and upper slope regions prominent gravitational collapse occurred above the basin-dipping decollement surfaces. This updip extensional movement is gradually accommodated by toe-thrust systems of lower slope regions (Figures 1a and 1b, after Wu et al. [2015]). The Niger deepwater toe-thrust systems can be subdivided into an inner and outer fold and thrust belts, which are linked by a translational zone featuring broad detachment folds with less deformed depocenters (Corredor et al., 2005). The study area of this paper covers an area of  $\sim 1,200$  km<sup>2</sup> in the southern lobe of the deepwater Niger Delta, between the outer fold and thrust belt and translational zone where a series of imbricate thrust faults and related folds developed (Figures 1a and 2). As these structures are closely related to the deformation of underlying shale units, this location is selected as a representative case from where to study the interactions between shale deformation and structural deformation within the sedimentary overburden.

The Niger Delta contains sedimentary strata from the Cretaceous to the Holocene overlying oceanic and fragments of continental crust (Figure 1c). The Cretaceous section is largely distributed in the delta-proximal area over continental crust. It consists of complex fluvial-shallow marine clastic sediments formed in the early rifting stage. The post-Paleocene deltaic succession is a thick seaward-prograding sedimentary wedge formed in the late drifting stage, which overlies oceanic crust in the distal area of the delta. Three diachronous lithologic formations have been divided for the Tertiary section of the Niger Delta, including (1) the basal Akata Formation of prodelta-marine shales; (2) the middle Agbada Formation of delta front and gravity flow complexes; and (3) the top Benin Formation of continentally sourced sands (e.g., Avbovbo, 1978). In the deepwater regions where the Benin Formation is absent, the thick, overpressured, marine shales of Akata Formation are commonly thought to be mobile in nature involving apparent deformation and multiple detachment levels (Bilotti & Shaw, 2005; Briggs et al., 2006; Cohen & McClay, 1996; Damuth, 1994; Maloney et al., 2010; Morley, 2003; Morley & Guerin, 1996). The overlying Agbada Formation composed of submarine channel-lobe complexes, debris flows and shales, represent the sedimentary overburden showing a variety of thrust-related structures. The thrusting deformation is still active today especially in the distal part of the outer fold-thrust belt, with bathymetric expression of structures at seafloor (Higgins et al., 2009; Jolly et al., 2016, 2017).

Previous work based on regional 2D or 3D seismic reflection data have demonstrated the basic tectono-stratigraphic characteristics in the deepwater Niger Delta (e.g., Bilotti & Shaw, 2005; Briggs et al., 2006; Corredor et al., 2005; Maloney et al., 2010; Rouby et al., 2011). The basement of Cretaceous oceanic crust is characterized by a set of faulted high-amplitude reflections buried over 5,000 ms two-way travel time (TWTT) beneath seafloor, which are overlain by a thick section of discontinuous, acoustically transparent reflections representative of homogenous marine shales of the Akata Formation (Figures 3a and 3b). Within the Akata Formation, three continuous high-amplitude reflections (X, Y, Z) have been recognized across the deepwater regions, which were interpreted as the major detachment levels (Figure 3b, Maloney et al., 2010). These marker reflections can be correlated with some interbedded sandy layers within the shale-dominated sequences, and represent thin-layered, bedding-parallel fault zones with severe fractures, high strain rate, and pore-fluid overpressure (Maloney et al., 2010; Morley et al., 2017). These features cause sharp decrease in acoustic velocities and form an impedance contrast displaying the continuous high-amplitude reflections. The marker reflection Y corresponds to the regionally continuous mid-Akata reflection that separates the upper less deformed Akata Formation from the lower greatly deformed Akata Formation (Corredor et al., 2005; Higgins et al., 2007). The shales between reflections Y and Z are thickened with incoherent

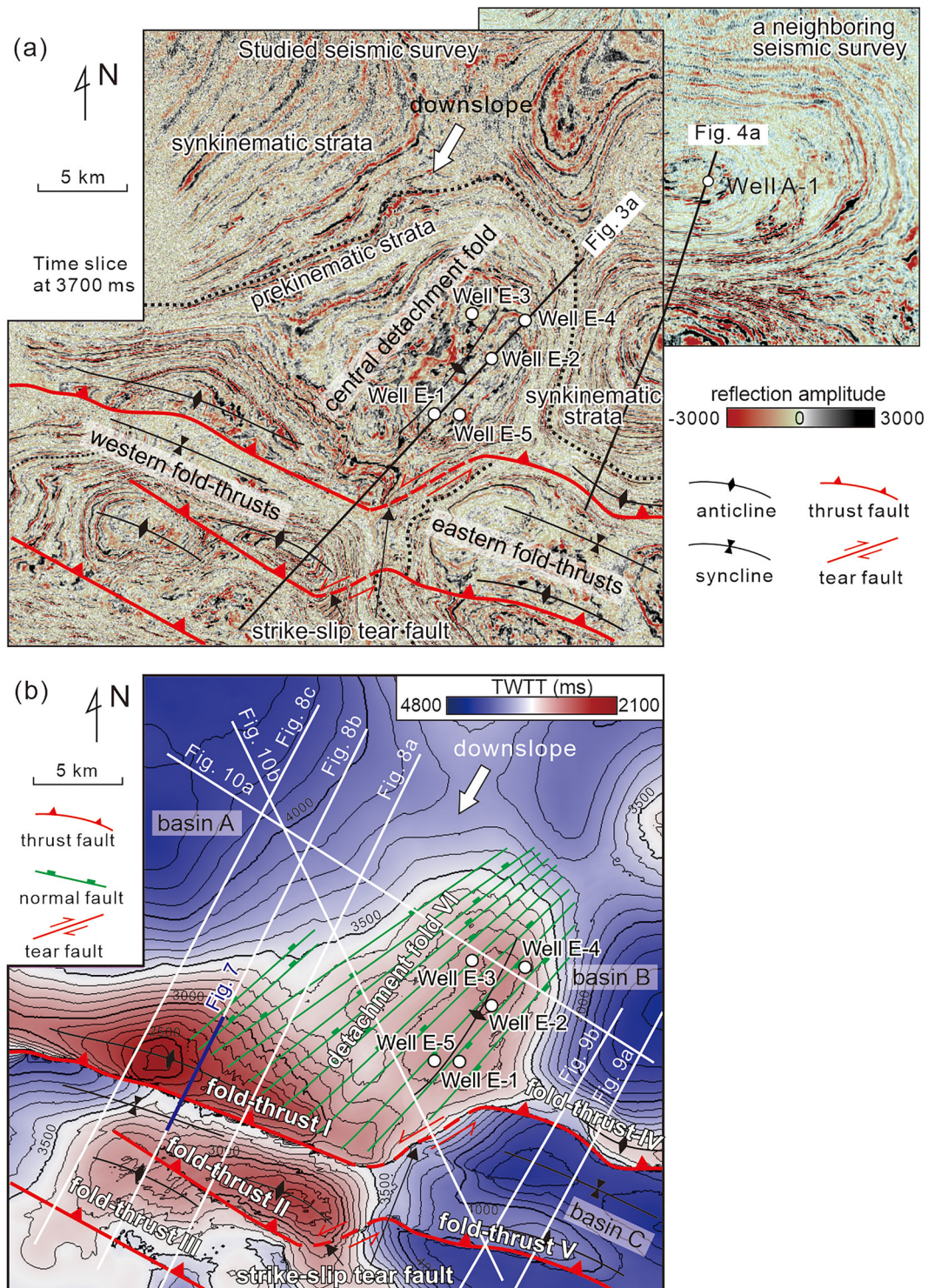
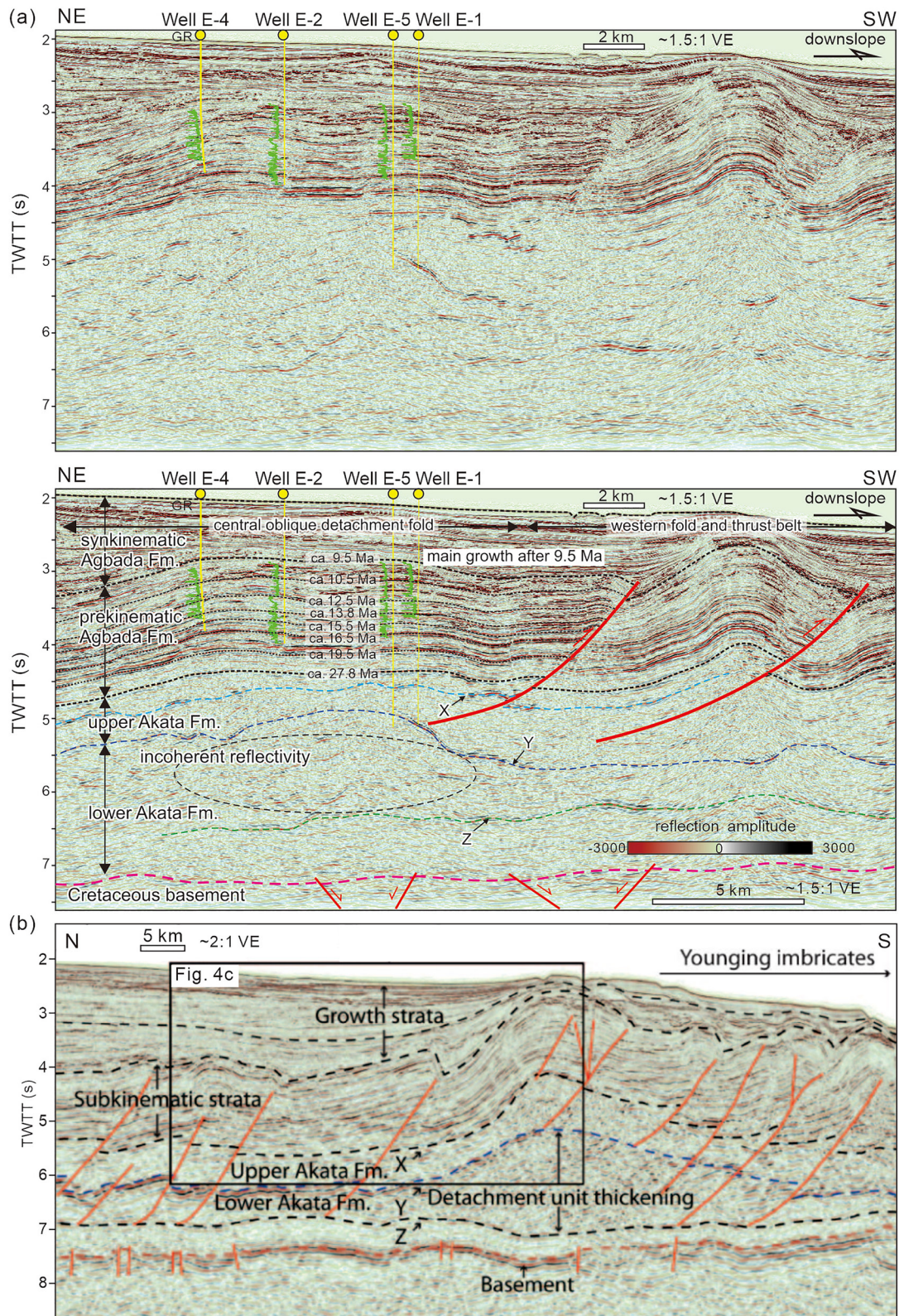


**Figure 2.** (a) Seismic time slice at 3,700 ms TWTT showing tectono-stratigraphic features over the study area. The black dashed line represents the 3,700 ms TWTT contour that separates the prekinematic strata (subparallel reflections) from the synkinematic strata (convergent reflections). The prekinematic strata is faulted and folded by several seaward-verging imbricate thrust faults, forming gravity-driven fold and thrust belt. There is a neighboring seismic survey with drilling wells northeast of the study area, which were used for stratigraphic correlation and well calibration. (b) Time structure map of the synkinematic-prekinematic boundary showing map-view structures over the study area. The western fold-thrusts (numbered I–III) and the eastern fold-thrusts (numbered IV–V) are laterally linked by sinistral strike-slip tear faults, and separated by a central detachment fold (numbered VI). These structures confine three piggyback basins (A, B, C). TWTT, two-way travel time.



reflectivity (Figure 3a), implying complex internal structures. The thickening of shales coincident with complex internal structures supports the assumption that the shale thick originates from tectonic deformation instead of a pre-tectonic, depositional shale thick. The precise ages of reflections X-Z are unknown due to the lack of wells penetrating the overpressured Akata shales.

Overlying the Akata Formation, the Agbada Formation is characterized by a thick package of semicontinuous high-amplitude reflections tied to interbedded sand-mud deposits in well logs (Figure 3a). Within the Agbada Formation, the upper wedge-shaped synkinematic section is clearly distinct from the lower prekinematic section which features subparallel strata with pronounced fold geometry. In the study area, eight seismic horizons have been identified in the prekinematic Agbada Formation (Zhang et al., 2016, 2018). According to seismic correlation with regional sequence stratigraphy and biostratigraphy across the basin (Fadiya & Salami, 2015; Henriksen et al., 2011; Krueger & Grant, 2011; Olayiwola et al., 2017), these horizons can be dated to ca. 27.8, 19.5, 16.5, 15.5, 13.8, 12.5, 10.5, and 9.5 Ma, respectively (Figure 3a). Thus, the main growth of gravity-driven structures started after ca. 9.5 Ma in the study area, nearly synchronous with adjacent regions (e.g., Pizzi et al., 2020). Within the late Miocene-to-present synkinematic Agbada Formation, several growth strata packages have been identified based on changing stratal geometries (Figure 4c), which were interpreted to represent different stages of structural growth evolution (Jolly et al., 2016; Krueger & Grant, 2011; Maloney et al., 2010).

Based on previously built tectono-stratigraphic framework (e.g., Corredor et al., 2005; Maloney et al., 2010; Zhang et al., 2018), this study focuses on the structural style of the prekinematic Agbada Formation overlying the deformed shale unit, through interpretation of multiple seismic sections. Subdivision and mapping of growth units within growth strata packages helps reconstruct the growth history of shale-related structures. Further analysis comparing various structural styles, spatiotemporal growth histories, and 3D interpretation of shale deformation can provide insight into the role of 3D shale deformation in the development of the deepwater gravitational system.

### 3. Data and Methods

The primary data used for tectono-stratigraphic interpretation are a 3D seismic reflection data provided by the China National Offshore Oil Company (CNOOC). It is a poststack time-migrated volume with a bin size of  $12.5 \times 12.5$  m and a vertical sampling rate of 3 ms. The data are displayed with “SEG normal polarity” where an increase in impedance is represented by peak reflectors. The shallow synkinematic section has a peak frequency of  $\sim 70$  Hz and a resulting vertical resolution of  $\sim 7$  m assuming an average interval velocity of 2,000 m/s, which could decrease to  $\sim 30$  Hz ( $\sim 25$  m) in the deep prekinematic section with the strata velocity increased to average 3,000 m/s (Figure 4b). The strata velocity averages about 2,600 m/s for the overpressured Akata shale (Maloney et al., 2010). Despite the generally increasing trend of seismic velocity with depth, it has been noted that there is only minimal change in the geometries of fault-related fold after depth conversion (Maloney et al., 2010). Thus, the seismic sections used here are all displayed in time domain, and the vertical exaggeration is calculated following the average velocity of target interval. Additionally, five wells (E1–E5) drilled to the prekinematic Agbada Formation ( $\sim 2,000$ – $3,000$  m below seafloor) have been tied to the seismic through synthetic seismogram. The gamma ray (GR) log calibrates the Agbada Formation to be a thick interbedded sand-mud clastic system consisting of multiple sedimentary sequences (Figure 3a). There is another well (A1) in the northeastern neighboring seismic survey with wireline logs in the shallow synkinematic section (Figures 2a and 4a), which was used for the well calibration of growth units associated with the growing structures.

**Figure 3.** (a) Uninterpreted and interpreted seismic profiles (see Figure 2a for the seismic line location) showing the general tectono-stratigraphic features across the study area. Three marker high-amplitude reflectors (X, Y, Z) are recognized within the Akata shales displaying notable deformations. The overlying Agbada Formation is subdivided into a prekinematic section and a synkinematic section based on the strata geometry. Well-to-seismic tie within the prekinematic section identified eight seismic horizons with chronological constraint (after Zhang et al. [2018]), and the main growth of gravity-driven structures started after ca. 9.5 Ma. TWTT = two-way travel time. Vertical exaggeration (VE) is  $\sim 1.5:1$  assuming a 3,000 m/s seismic velocity. (b) Regional seismic profile west of the study area (see Figure 1a for the seismic line location) showing comparable tectono-stratigraphic features in the southern lobe of the Niger Delta, modified from Maloney et al. (2010). The Agbada Formation features prominent thrusting and folding deformation underlain by thickened Akata shales.

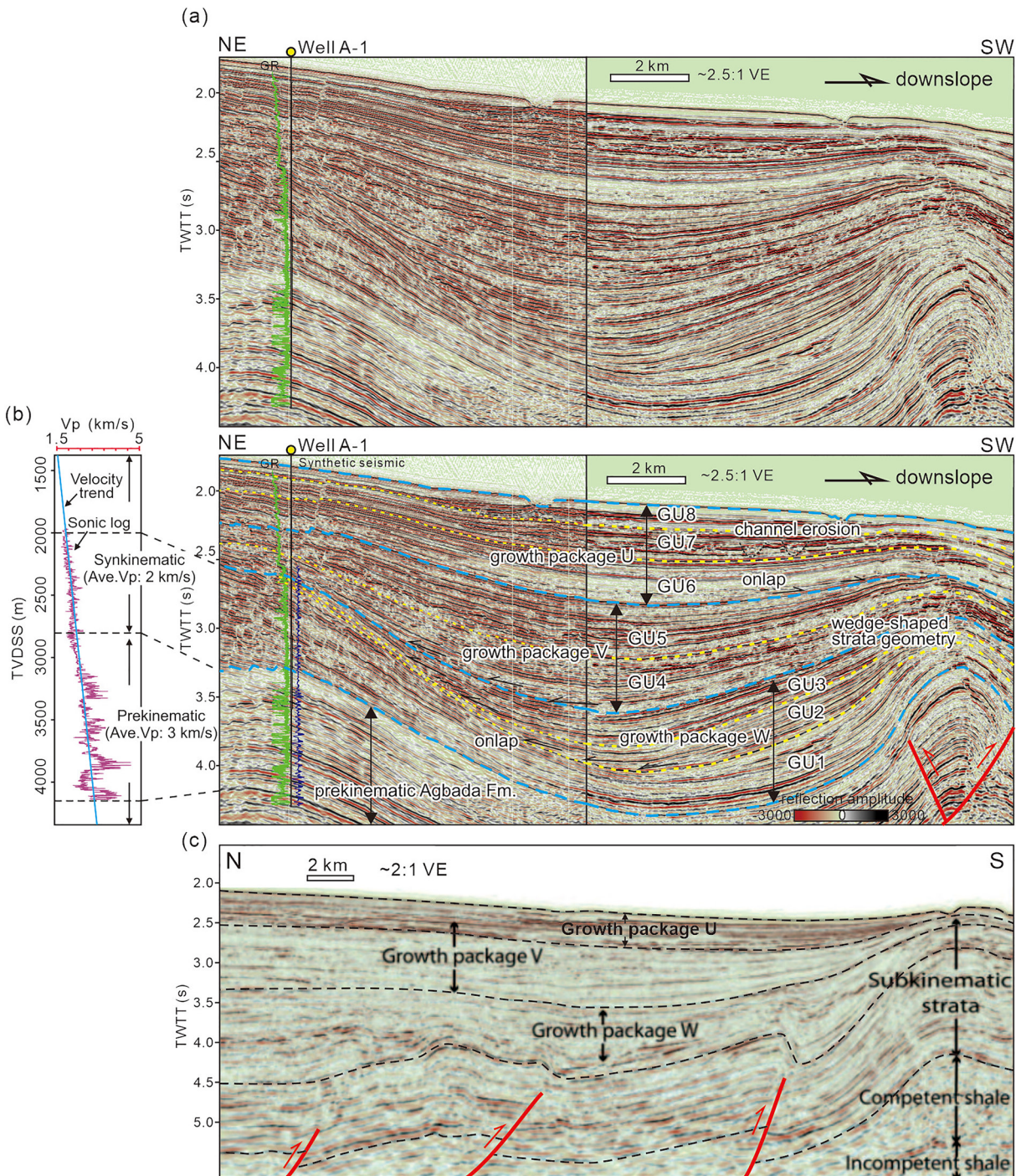


**Figure 4.** (a) Uninterpreted and interpreted seismic profiles correlated with a neighboring seismic survey and drilling well (see Figure 2a for the seismic line location), showing the division of growth units within the synkinematic Agbada Formation. The synkinematic section consists of three growth strata packages (W, V, U), which are subdivided into eight growth units (GU1–GU8) based on angular unconformity and contrasting seismic facies across the bounding surfaces. TWTT = two-way travel time. Vertical exaggeration (VE) is ~2.5:1 assuming a 3,000 m/s seismic velocity. (b) Strata velocity derived from sonic logs of Well A-1. The average velocity is ~3,000 m/s for the prekinematic strata, and ~2,000 m/s for the synkinematic strata. (c) Seismic profile west of the study area (inset section from Figure 3c) showing comparable features of growth strata packages (W, V, U), modified from Maloney et al. (2010).



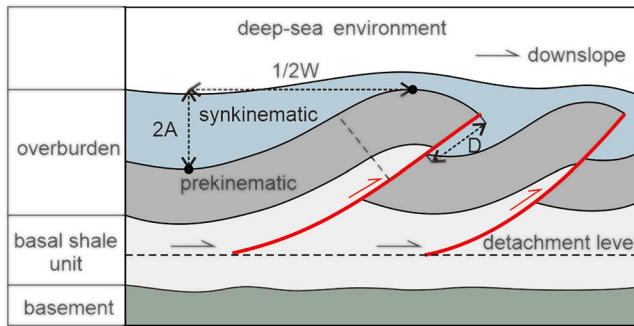


**Figure 5.** Basic terminologies used for the description of structures in the study area. The geometry of thrust-related folds is quantitatively described by measuring the horizontal and vertical distance between the anticline and syncline hinge points, which amount to the half of fold wavelength ( $W$ ) and double fold amplitude ( $A$ ), respectively.  $D$  = thrust fault displacement.

Seismic interpretation in this study is based on the Geophysics module from the Schlumberger's Petrel interpretation software, in which both the 3D seismic data set and wireline logs were loaded. Seismic profiles and time slices were combined to carry out detailed structural interpretation. The major thrust faults and related crestal normal faults were interpreted in seismic reflection profiles based on apparent strata offset across the fault planes, and time slices help to determine the fault traces and configuration relationship between faults (Figure 2a). Some key structural marker reflections were picked in a loose grid of  $100 \times 100$  traces and then interpolated throughout the volume to generate 3D mapped horizons, including the seabed, synkinematic-prekinematic boundary, three marker reflections ( $X$ ,  $Y$ ,  $Z$ ) within the Akata shales, and the basement top. The time structure map of synkinematic-prekinematic boundary overlain with fault traces was mapped over the study area to reveal the spatial distribution of thrust-related structures (Figure 2b). Geometric parameters, such as fold wavelength ( $W$ ), fold amplitude ( $A$ ), and fault displacement ( $D$ ), were measured on the synkinematic-prekinematic boundary to quantitatively analyze the intensity of structural deformation within the overburden. Since the thrust-related folds are generally

asymmetrical in cross sections, we define the horizontal and vertical distance between anticline and syncline hinge points as half of fold wavelength and double fold amplitude, respectively (Figure 5). With no accurate 3D velocity model available, the geometric parameters measured in time domain were converted to depth using an average 3,000 m/s velocity for the prekinematic strata, according to the sonic log (Figure 4b). The uncertainty for calculated geometric parameters, especially fold amplitude and fault displacement, mainly arises due to changing velocities between measured points, estimated to be within 200 m/s and potentially causing error within 50 m. This error is considered to have very limited impact on either the fold geometries or the relative deformational intensity between thrust-related folds.

Seismic stratigraphic interpretation builds on previous work on synkinematic strata architecture from an adjacent survey (Maloney et al., 2010, see the survey location in Figure 1a), where three growth packages ( $V$ ,  $W$ ,  $U$ ) have been identified (Figure 4c). As no seismic lines directly connect our study area with Maloney's study area, stratigraphic correlation between these two surveys was conducted based on the prominent strata geometries of the three growth packages: (1) the oldest growth package  $W$  shows a high-angle strata wedge with apparent strata rotation and unconformities flanking the thrust-related folds; (2) the middle growth package  $V$  shows a gradually thinning strata wedge that onlaps toward the fold crest; (3) the youngest growth package  $U$  overlaps and thins onto the fold crest with notable channel erosion. Within all three growth packages, we identified seven angular unconformities (onlapping or truncation) near the fold crest that transition into conformities away from structural highs (Figure 4a). Across these unconformities, abrupt changes in seismic facies and lithological cycles (Figure 4a) suggest notable changes in the relationship between sediment accumulation rate and structural growth rate. We picked these seven unconformities in a loose grid of  $200 \times 200$  traces then interpolated them throughout the study area. The resulting seismic horizons constitute eight growth units (GU1–GU8) within the synkinematic Agbada Formation (Figure 4a). An analysis of varying strata geometries within different growth units (Figure 6), such as the features of strata rotation in response to growing structures (Figure 6b), improves our understanding of the structural growth evolution in space and time. Considering local strata erosion from submarine channel bypassing or mass-transport sliding (Figure 7a), the growth unit horizons were reconstructed by extrapolating along the structural trend (Figure 7b). These reconstructed horizons were then subtracted from each other to generate TWTT thickness, or isochron maps for each growth unit, which approximate the paleotopography prior to deposition of each growth unit.

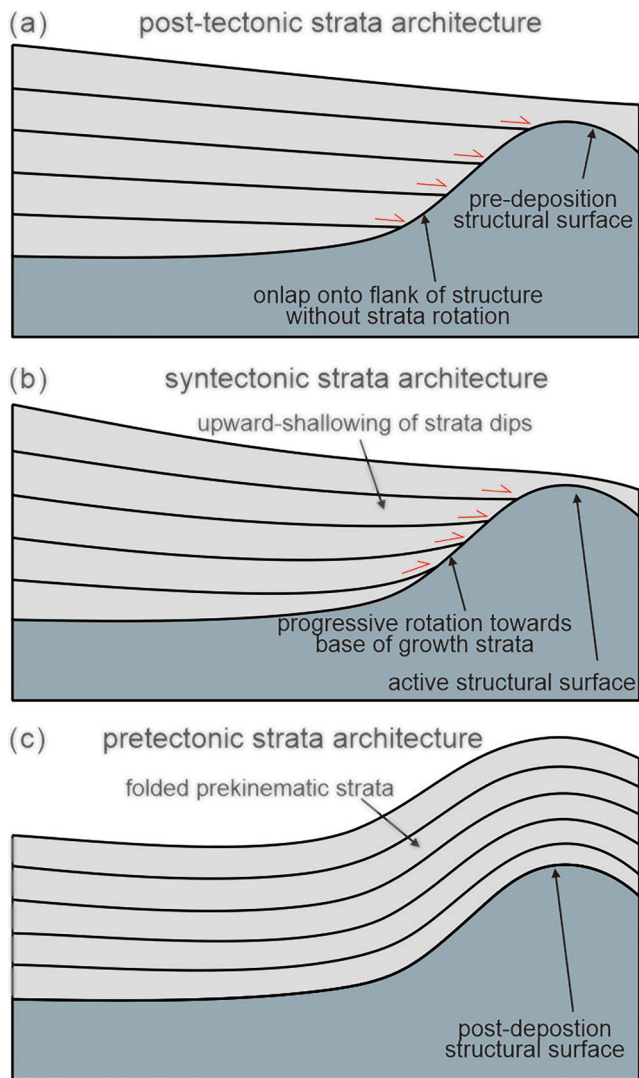


**Figure 6.** Conceptual model illustrating the varying strata geometries at different structural scenarios. The syngrowth strata features apparent rotation with upward-shallowing of strata dips (b), contrasting with the passive onlap without strata rotation for the predeposition structure (a). The pregrowth strata are subparallel and folded without apparent strata thinning over the fold crest (c).

#### 4. Structural Style of the Deepwater Gravitational System

In this section, we mainly use 3D tracked seismic horizons together with multiple seismic sections to describe the varied structural styles within the prekinematic strata. The mechanisms by which various structural styles formed are addressed in Section 6 with the integration of strong evidences. According to the time structure map of the top prekinematic horizon (Figure 2b), structures in the study area can be divided into three parts: (1) the western study area consists of three major subparallel fold-thrusts trending WNW to ESE, numbered I–III; (2) the eastern study area consists of two major subparallel fold-thrusts trending WNW to ESE, numbered IV–V; (3) the central study area features an NE–SW-trending anticline oblique to the strike of major thrust faults, numbered VI. These three structural parts are spatially connected and confine three piggyback basins in the hanging wall of thrust faults, named A, B, and C (Figure 2b). These three basins are filled with synkinematic strata showing convergent reflections on time slice (Figure 2a), clearly distinguished from parallel reflections of prekinematic strata within the fold core. The following interpretation of multiple seismic sections that cross different parts of the study area provides more details about structural style of the deepwater gravitational system.

##### 4.1. Western Study Area: Shale-Cored Fold-Thrusts

Strike-normal seismic profiles show prominent deformation in both the prekinematic strata and basal shale unit in the western study area (Figures 8a–8c). The prekinematic strata is faulted and folded by three major seaward-verging imbricate thrust faults (I–III) that extend upsection into the bottom of synkinematic strata and die out downsection into the middle of the basal shale unit. The major imbricate thrust faults are joined by minor landward-verging thrust faults in the hanging wall. The basal shale unit beneath the fold crest thickens apparently involving marker reflections Y and Z. The upper reflection Y, which is partly offset by three major thrusts at low angles, trends parallel to the overlying folded prekinematic strata, with shales above reflection Y being weakly deformed. The lower reflection Z is subhorizontal and parallel to the oceanic basement, with less deformed shales below reflection Z. It is the shales between reflections Y and Z that are greatly deformed with wedge-shaped geometry and primarily contribute to thickening of the basal shale unit. Overall, large thrusts and folds overlying a thickened shale core characterize the western study area.

The shale-cored fold-thrusts observed in the western study area may fall into different fault kinematic models depending on interpretation of thrust faults. Uncertainty regarding the downward termination of thrust faults exists due to the general weak reflections within the basal shale unit. If thrust faults are interpreted to extend deep into the master detachment level, like in Figure 3b (Maloney et al., 2010), it should belong to fault-propagation folds. Another interpretation is the shallower extension of thrust faults that are separated from the master detachment level, as done in this study, which may fit with the model of break-thrust style fold where major thrusts propagate downward before reaching the master detachment level (Morley, 2009; Morley & Naghadeh, 2018; Morley et al., 2017). Despite such uncertainty in fault interpretation, our main concern is how shale thickening has progressed during the process of thrusting and folding, which is detailed in Section 6.

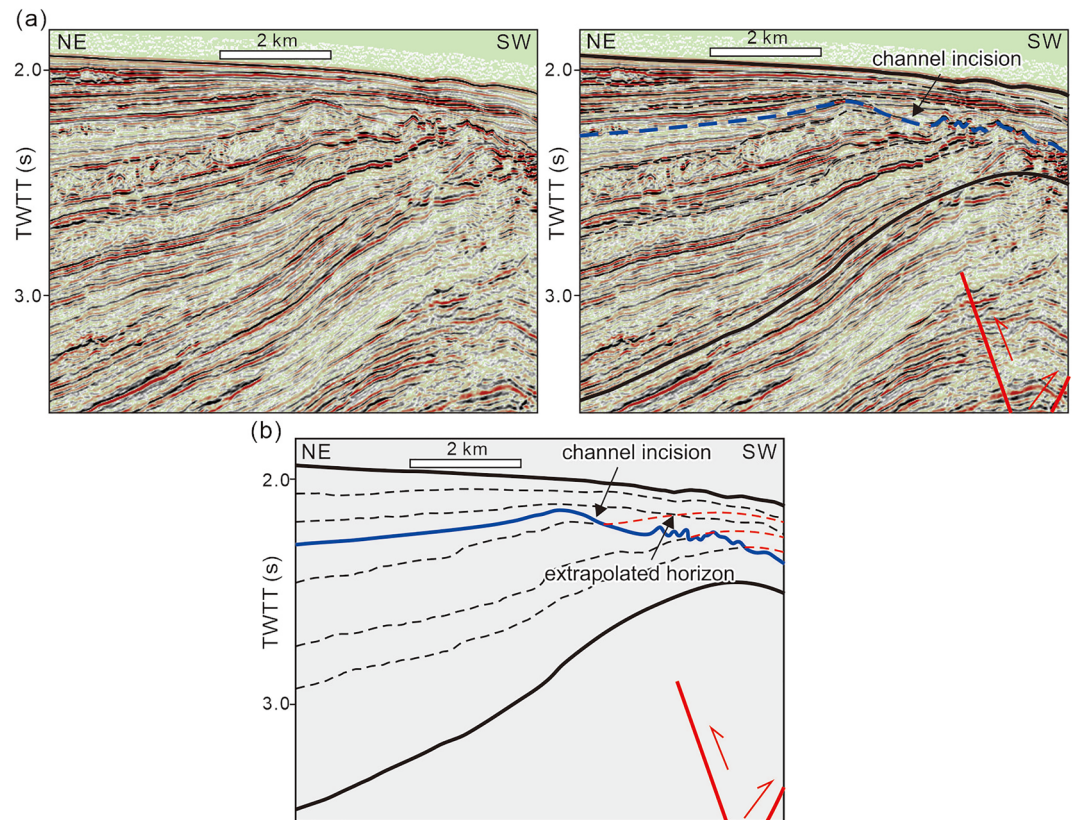


**Figure 7.** (a) Uninterpreted and interpreted seismic profiles (see Figure 2b for the seismic line location) showing the local erosion of strata over the fold crest. (b) Reconstruction of eroded horizons. The horizons were extrapolated following the structural trend before generating the isochron maps.

Comparison between different reflection profiles shows that fold geometries within the overburden and deformation within the basal shale unit vary along structural strike. Across the central fold-thrusts (Figure 8c), the fold deformation in the hanging wall exhibits concave-up geometry without apparent thickening in the basal shale unit, and there is limited occurrence of lower marker reflection Z in the profile. As the positions of reflection profiles change to the eastern side of thrusts near the central detachment fold (Figures 8a and 8b), the fold geometries transition into slightly concave up accompanied by apparent shale thickening between marker reflections Y and Z, and the lower marker reflection Z extends much longer in the profiles. These changes suggest increased impact of shale deformation on the thrusting and folding deformation. The along-strike changes in fold geometries are also manifested by changes in quantitative geometric parameters; while the fold amplitude of fold-thrust I decreases eastward from  $\sim 0.7$  to  $\sim 0.5$  km and the fold wavelength of fold-thrust I increases eastward from  $\sim 20$  to  $\sim 36$  km (Table 1). The fault displacement of fold-thrust I decreases eastward from  $\sim 1$  to  $\sim 0.4$  km, suggesting the gradual weakening of thrusting intensity toward the margin of thrust faults.

#### 4.2. Eastern Study Area: Fold-Thrusts Without Shale Core

Strike-normal reflection profiles across the eastern study area show that the structural deformation mainly occurs in the prekinematic strata with less thickness changes within the basal shale unit (Figures 9a and 9b). Two major seaward-verging imbricate thrusts (IV–V) completely fault the prekinematic strata creating prominent anticlines in the hanging wall that is locally faulted by minor landward-verging thrusts. The major fault-plane reflections cut downsection through the marker reflection X near the top of basal shale unit at low angles. This reflection X is not clear in the western study area. The marker reflection Z is also observed in the middle of basal shale unit which laterally extends into the western study area

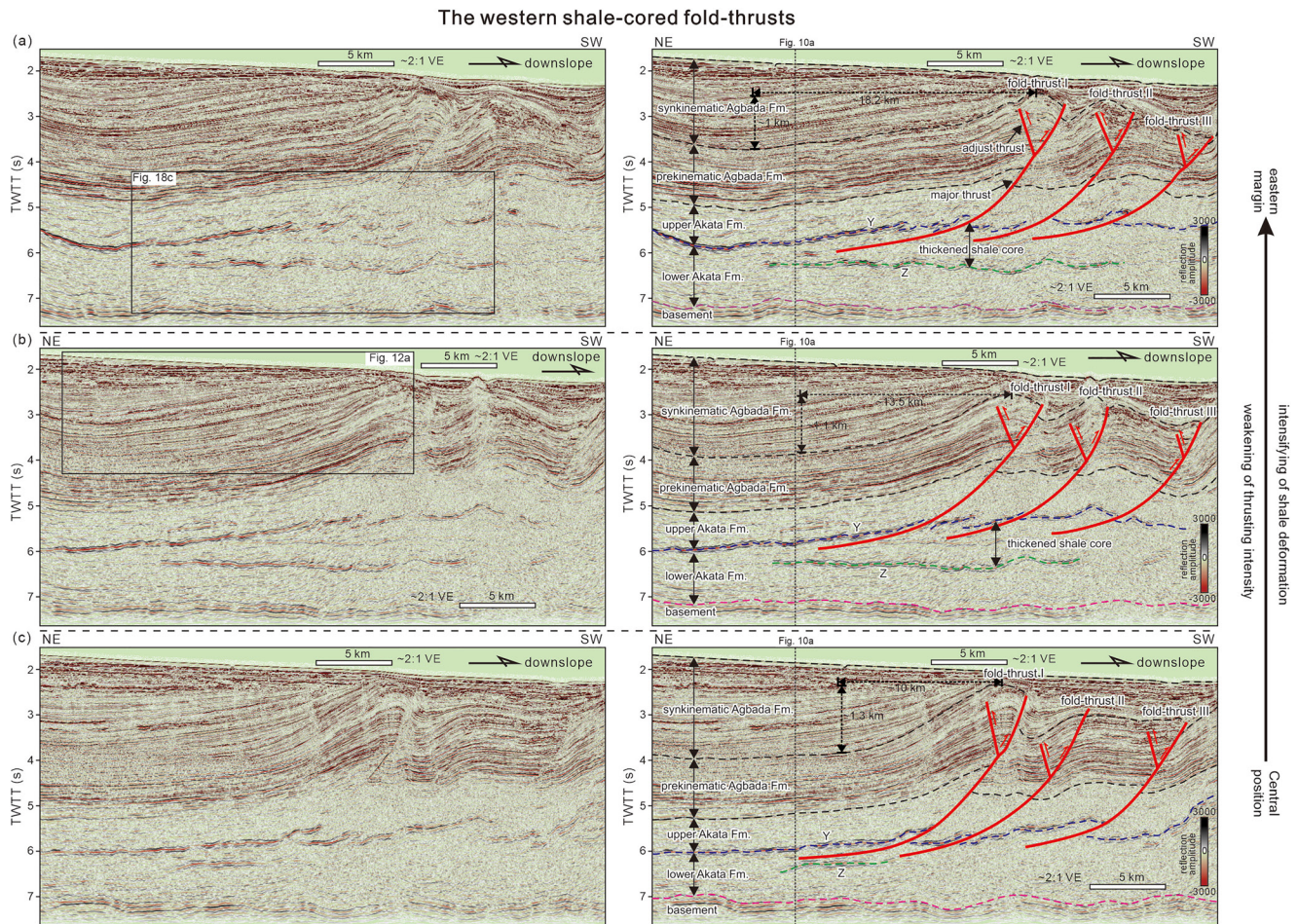


**Figure 8.** Uninterpreted and interpreted seismic reflection profiles across the western study area (see Figure 2b for the seismic line location) showing the deformation characteristics of shale-cored fold-thrusts. From the central position (c) to the eastern margin (b, a) of the fold-thrusts, the basal shale unit thickens gradually between marker reflections Y and Z, with varied fold geometry and fault displacement in the prekinematic strata. TWTT = two-way travel time. Vertical exaggeration (VE) is  $\sim 2:1$  assuming a 3,000 m/s seismic velocity.

(Figure 10). The reflection X and Z are nearly parallel to each other without apparent changes of shale thickness between them. Overall, simple fold-thrusts without shale core characterize the eastern study area.

As compared to the shale-cored fold-thrust I in the western study area (Figure 8), the laterally adjacent fold-thrust IV in the eastern study area exhibits lower strain with the fold amplitude ranging from  $\sim 0.2$  to  $\sim 0.4$  km, fold wavelength ranging from  $\sim 6$  to  $\sim 11$  km, and fault displacement ranging from  $\sim 0.4$  to  $\sim 0.7$  km (Table 1). Such different deformational intensity is also seen visually on the map (Figure 2b), suggesting that the western fold-thrusts experienced larger contractional shortening than the eastern fold-thrusts. The change in structural styles between the eastern and western fold-thrusts is assumed to be related to 3D shale thickness variation, which is detailed in Section 6.

#### 4.3. Central Study Area: Oblique Detachment Fold

Strike-oriented seismic profiles across the oblique anticline VI in the central study area show prominent deformation in both the prekinematic strata and basal shale unit (Figure 10). The prekinematic strata is asymmetrically folded without direct connection to major thrusts. Compared to the broad gentle western limb, the eastern limb is much steeper with a notable synclinal geometry. The full fold geometry has a wavelength of  $\sim 30$  km and an amplitude of  $\sim 0.6$  km (Table 1), equivalent to the scale of the western fold-thrusts. Both limbs of the anticline VI are cut by two sets of NE-SW-trending normal faults with opposite

**Table 1**  
*Summary of Structural Deformation at Different Positions of the Target Deepwater Gravitational System*

Fold and thrust belt		Deformational features	Maximum thickness of basal shale unit (km) <sup>a</sup>	Geometric parameters (km) <sup>b</sup>		
				W	A	D
Western fold-thrusts (I–III)	Profile a (eastern margin, Figure 8a)	Shale-cored fold-thrusts with slightly convex-up fold geometry in the hanging wall	3.7	36	0.5	0.4
	Profile b (eastern margin, Figure 8b)	Shale-cored fold-thrusts with slightly concave-up fold geometry in the hanging wall	3.8	27	0.6	0.5
	Profile c (central position, Figure 8c)	Fold-thrusts without thickened shale core, apparent concave-up fold geometry in the hanging wall	3.1	20	0.7	1.0
Eastern fold-thrusts (IV–V)	Profile a (central position, Figure 9a)	Fold-thrusts without thickened shale core, apparent concave-up fold geometry in the hanging wall	2.5	11	0.4	0.7
	Profile b (western margin, Figure 9b)	Fold-thrusts without thickened shale core, slightly concave-up fold geometry in the hanging wall	2.6	6	0.2	0.4
Central oblique detachment fold (VI)	Profile a (central position, Figure 10a)	Asymmetrical shale-detachment fold cut by tiers of crestal normal faults, thinning of shales beneath the eastern limb	3.9	30	0.6	—
	Profile b (southern margin, Figure 10b)	Asymmetrical shale-detachment fold longitudinally bound by strike-slip tear faults	3.8	26	0.5	—

<sup>b</sup>The geometric parameters were measured for fold-thrust I in the western study area, fold-thrust IV in the eastern study area, and detachment fold VI in the central study area. Time-depth conversion was conducted using a constant 3,000 m/s velocity. W = fold wavelength; A = fold amplitude; D = thrust fault displacement. <sup>a</sup>The shale thickness is calculated using a 2,600 m/s seismic velocity.

dip (Figure 2b), which display tiers of closely spaced normal faults in cross section (Figures 10a and 10c). These two sets of normal faults are localized to the fold crest (Morley, 2007), and can extend downward near the top of the basal shale unit without a neutral surface, suggesting the nature of bending folding that created local extension over the fold crest. Some of the crestal normal faults can extend upsection into the modern seafloor, indicating that they are still active today. The basal shale unit beneath the fold crest features a thickened shale core with three marker reflections (X, Y, Z) (Figures 10a and 10b). The upper reflection X is recognizable in the eastern limb and dies out gradually toward the fold crest. The middle reflection Y trends parallel to the western limb and dies out near the fold crest. The lower reflection Z trends parallel to the oceanic basement and extends all the way from eastern to western limb. The reflections Y and Z overlap mostly beneath the western limb, and the shale interval between reflections shows a wedge-shaped geometry that leads to the shale unit thickening from ~1,900 to ~3,000 ms in TWTT thickness. Beneath the eastern limb, the shale unit thins on average ~1,700 ms in TWTT thickness. The shale core beneath the central oblique anticline VI corresponds to the shale core beneath the western fold-thrusts (Figures 8a and 8b), suggesting a close relationship between these structures.

Considering the link between shale thickness variation and overlapping of reflections Y and Z, as well as incoherent reflectivity within the shale core, it is argued that the shale thick should originate from tectonic deformation of the depositionally isopachous shale unit, rather than from a pre-tectonic, depositional shale thick. Thus, the folding deformation overlying the thickened shale unit is interpreted as the shale-detachment fold, and reflection Z presumably serves as the master detachment. The oblique orientation of this detachment fold in map view (Figure 2b) suggests that structural shortening primarily occurred oblique or perpendicular to the regional slope. This paper describes the detachment fold as an oblique detachment fold in order to distinguish it from the typical detachment folds directly caused by downslope gravitational contraction (Epard & Groshong, 1995).

Map view of the central oblique detachment fold (Figure 2b) shows a longitudinal boundary by an oblique fault that laterally links the western and eastern fold-thrusts. The root mean square (RMS) amplitude map extracted within the prekinematic sequence shows the lateral displacement of the pre-tectonic submarine channel by the oblique fault (Figure 11). This provides evidence that the fault displacement has a significant strike-slip component. These kinds of oblique strike-slip faults between thrust faults are also known as

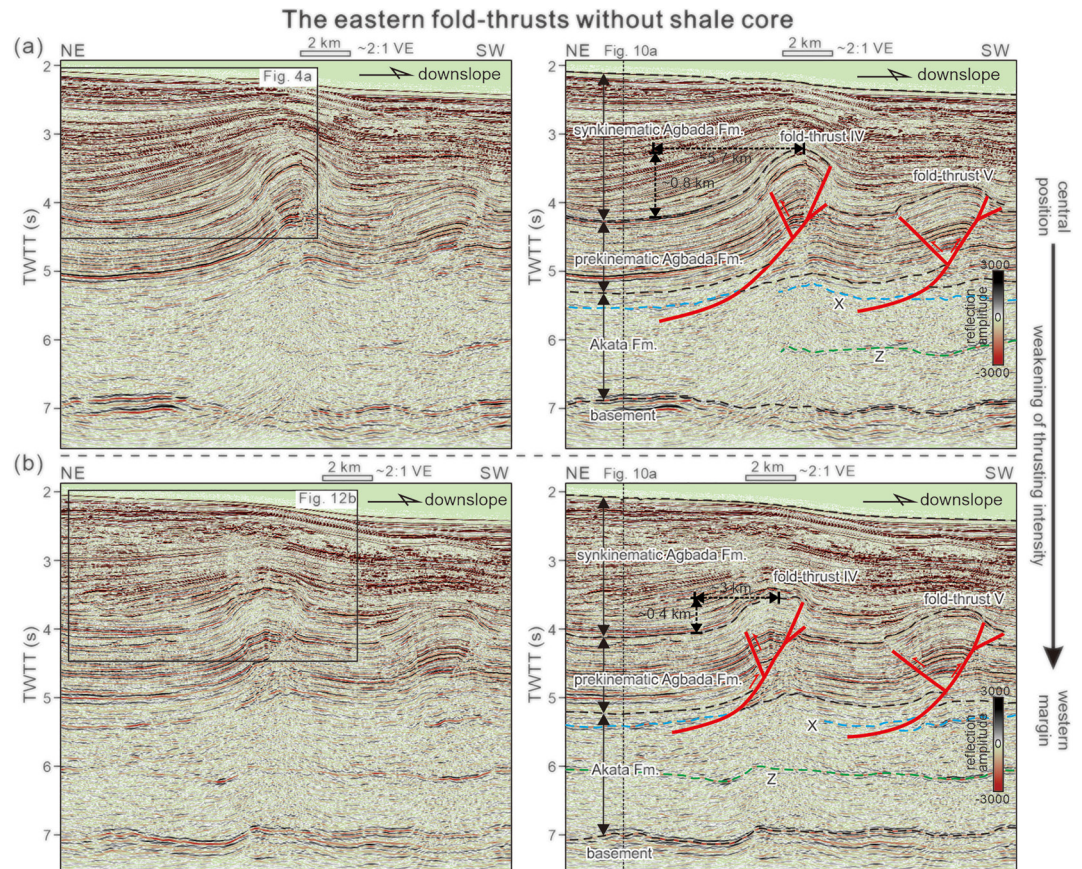


**Figure 9.** Uninterpreted and interpreted seismic reflection profiles across the eastern study area (see Figure 2b for the seismic line location) showing the fold-thrusts without shale core. The thrust faults terminate below marker reflection X without apparent thickening in the basal shale unit. The deformation degree and fault displacement decrease from the central position (a) to western margin (b). TWTT = two-way travel time. Vertical exaggeration (VE) is ~2:1 assuming a 3,000 m/s seismic velocity.

tear faults (e.g., Benesh et al., 2014; Mueller & Talling, 1997), and they have been widely recognized in the deepwater Niger Delta (Figure 1a) as a result of differential radial spreading of the delta (Wu et al., 2015). In addition to the strike-slip displacement, this oblique fault also has a dip-slip component exhibiting high-angle thrust fault in cross section (Figure 10d). This suggests that the oblique tear faults may be part of the two sets of thrust faults that were later displaced by the southwestward propagation of detachment fold VI along its strike.

## 5. Evolution History of the Deepwater Gravitational System

In this section, we focus on the evolution history of the deepwater gravitational system through seismic stratigraphic interpretation within the synkinematic strata, which allows understanding of the modern structural style in the prekinematic strata. Three growth packages, namely W, V, and U upsection, are recognized within the synkinematic strata. Each growth package is composed of multiple growth strata units showing varied geometries and thickness distribution, which generally reflects three episodes of tectonic evolution through time.

### 5.1. Growth Package W (GU1-GU3): Coevolution Between Thrusting and Shale Detachment Folding

The lower growth package W exhibits a set of moderate-amplitude, sheet-like reflections that thin and onlap onto the fold crest with wedge-shaped geometries distinguished from the underlying subparallel

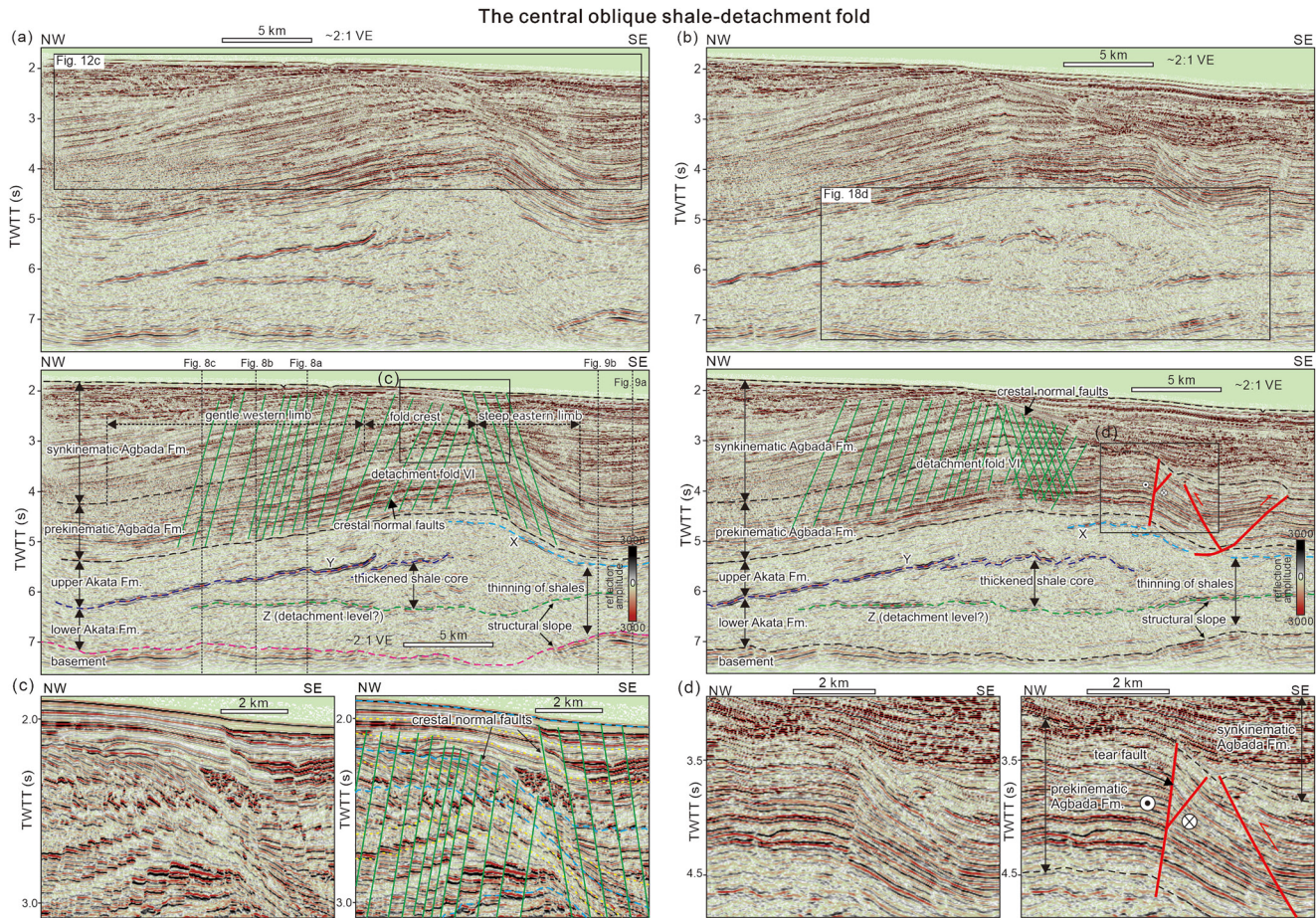


**Figure 10.** Uninterpreted and interpreted seismic reflection profiles across the central study area (see Figure 2b for the seismic line location) showing the deformation characteristics of oblique detachment fold. The oblique fold VI features asymmetrical geometry with a steeper eastern limb compared to the western limb (a). Underneath the fold crest and western limb develops thickened shale core between marker reflections Y and Z, contrasting with thinning of shales underneath the eastern limb (a, b). (c) Inset section from (a) showing tiers of closely spaced normal faults over the crest of detachment fold. The oblique detachment fold is longitudinally bounded by an oblique strike-slip tear fault which displays a high-angle thrust fault in cross section (d, inset section from b). TWTT = two-way travel time. Vertical exaggeration (VE) is ~2:1 assuming a 3,000 m/s seismic velocity.

prekinematic reflections (Figure 12). This package records deposition as the gravity-driven structural deformation initiated. The thickest parts away from structural highs indicate the depocenters of piggyback basins. Three component growth units (GU1–GU3) are recognized within growth package W which features apparent onlaps onto the fold limbs and indicate at least three episodes of sediment filling. Upward-shallowing of strata dips is clearly observed within the growth units, indicative of high growth rate with respect to the sediment accumulation rate during the growth package W (Figure 6b). Over the crest of the high-relief fold-thrusts in the western study area, growth package W is largely eroded by younger submarine channels (Figure 12a), a phenomenon not seen in the lower-relief fold-thrusts in the eastern study area (Figure 12b). Across the central oblique detachment fold (Figure 12c), the fold crests and depocenters gradually migrate northwest from GU1 to GU3, reflecting asymmetrical uplift in the western limb of the oblique detachment fold.

Erosion-reconstructed isochron maps for GU1–GU3 (Figures 13a–13c) reveal main thrusting coevolved with the oblique detachment fold as growth package W was being deposited. At the early time of GU1 (Figure 13a), the major thrusts largely formed in both the western and eastern study areas together with high-relief folding deformation in the hanging wall. Growth unit thickness varies greatly across the fault traces resulting in the elongated basin C between imbricate thrusts. In the meantime, the central oblique detachment fold initiated near the lateral linkage zone between thrusts with a narrow fold crest, which laterally separated the western basin A from the eastern basin B in the hanging wall of thrust faults. As

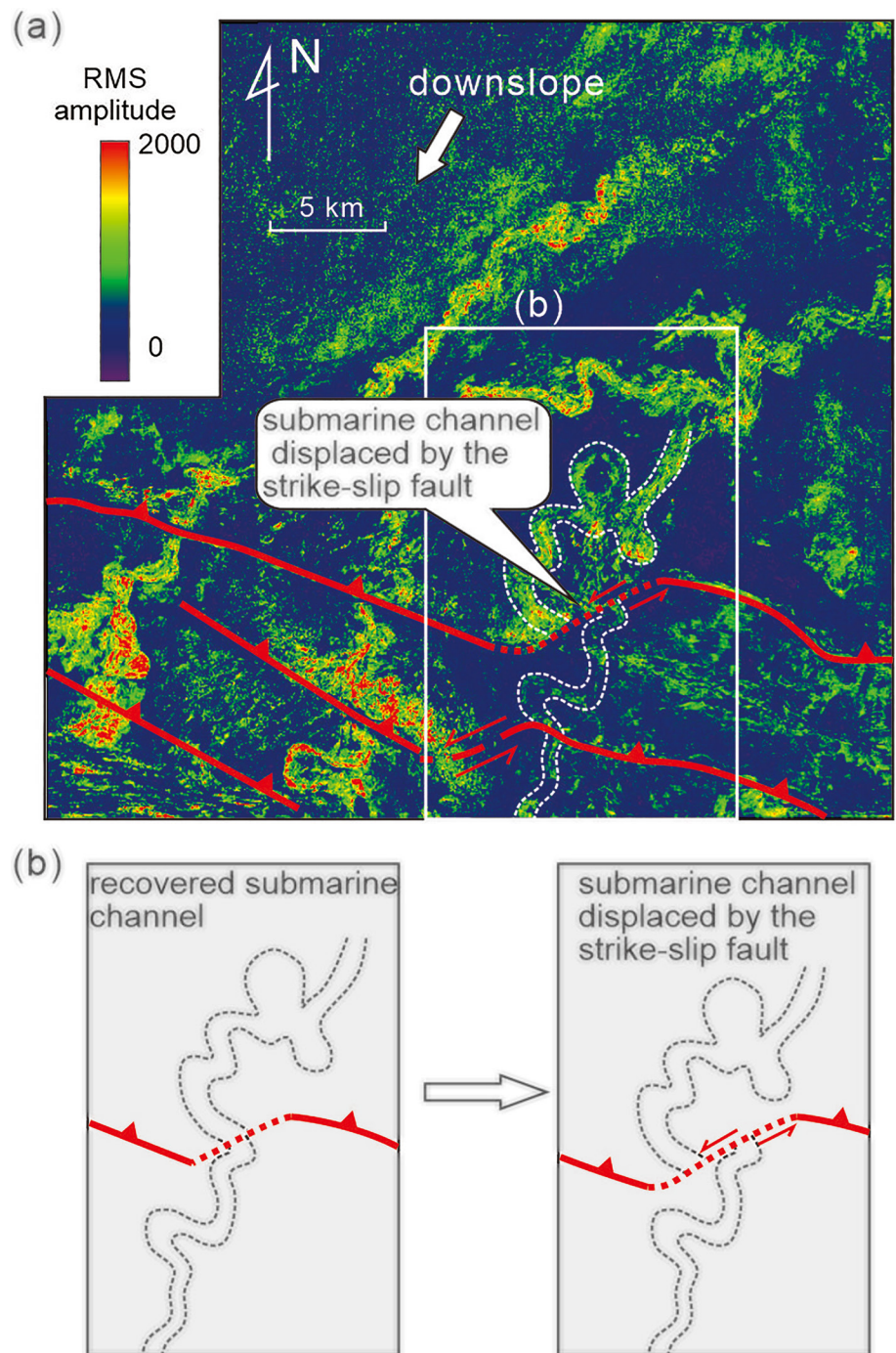


**Figure 11.** (a) Root mean square (RMS) amplitude map extracted within the prekinematic sequence, showing lateral displacement of the submarine channel by the strike-slip tear fault. (b) Reconstruction of the pre-tectonic submarine channel.

GU1 evolved into GU2 and GU3 (Figures 13b and 13c), structural relief of the main fold-thrusts reduces gradually and basin C become less recognizable, indicating that the downslope thrusting intensity weakened gradually through time. In contrast, the central oblique detachment fold extends longer to the upslope and across the downslope fold-thrust belt as well, resulting in the eastern and western fold-thrusts laterally separated. The detachment fold axis migrates to the northwest with the fold limbs rotating asymmetrically, which corresponds to the northwestward-migration features observed in seismic profile (Figure 12c). As a



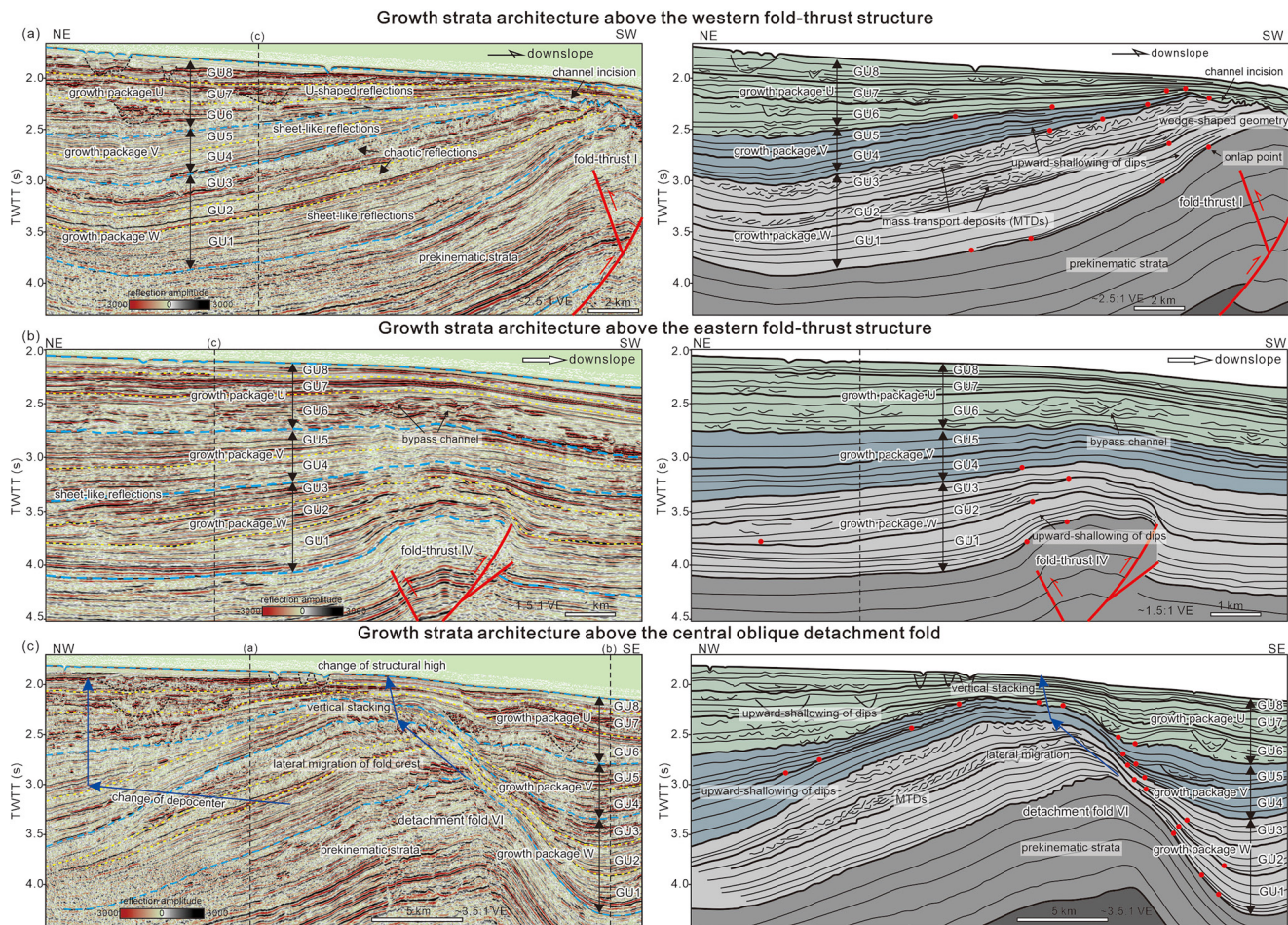


**Figure 12.** Seismic stratigraphic interpretation across the western fold-thrust structure (a, inset map from Figure 8b), the eastern fold-thrust structure (b, inset map from Figure 9b), and the central detachment fold (c, inset map from Figure 10a), showing varied strata architecture within the synkinematic section. Syngrowth strata over the western fold-thrusts is affected by mass-transport deposits and local channel incision. Growth units within the lower growth package W (GU1–GU3) feature lateral migration of structural highs and depocenters, which transitions into vertical stacking features for the upper growth package V (GU4–GU5) and U (GU6–GU8). TWTT = two-way travel time. Vertical exaggeration (VE) is  $\sim 2.5:1$  (a),  $1.5:1$  (b), and  $\sim 3.5:1$  (c) assuming a 3,000 m/s seismic velocity.

result, the western fold-thrusts partly merged with the central detachment fold at time of GU3 forming the shale-cored fold-thrusts observed in seismic profiles (Figures 8a and 8b). Over the western study area two sets of chaotic weak reflections with internal block rotation are observed in GU2 and GU3 (Figure 12a), representing mass-transport deposits (MTDs) (e.g., Gong et al., 2014; Morley, 2009; Moscardelli & Wood, 2008). These MTDs are assumed to be of intrabasinal origin (e.g., Heinio et al., 2006; Madof et al., 2009) with short distance of sliding and slumping, associated with the remobilization of unconsolidated deposits triggered by intense structural uplift of the detachment fold.

## 5.2. Growth Package V (GU4–GU5): Dominant Shale Detachment Folding

The middle growth package V is a set of moderate-to-low-amplitude, sheet-like reflections which show gentle strata wedge with depocenters diverted away from the underlying growth package W (Figure 12). The migration of depocenters suggests that the paleotopography has changed a great deal from growth package W to V. The gentle strata wedge thinning from the depocenters to the fold crest reflects moderate growth rate with respect to the sediment accumulation rate during growth package V. A low-angle onlap unconformity is identified near the fold crest which defines two component growth units (GU4–GU5) within growth package V. These units are eroded by younger incisional channels crossing the high-relief fold

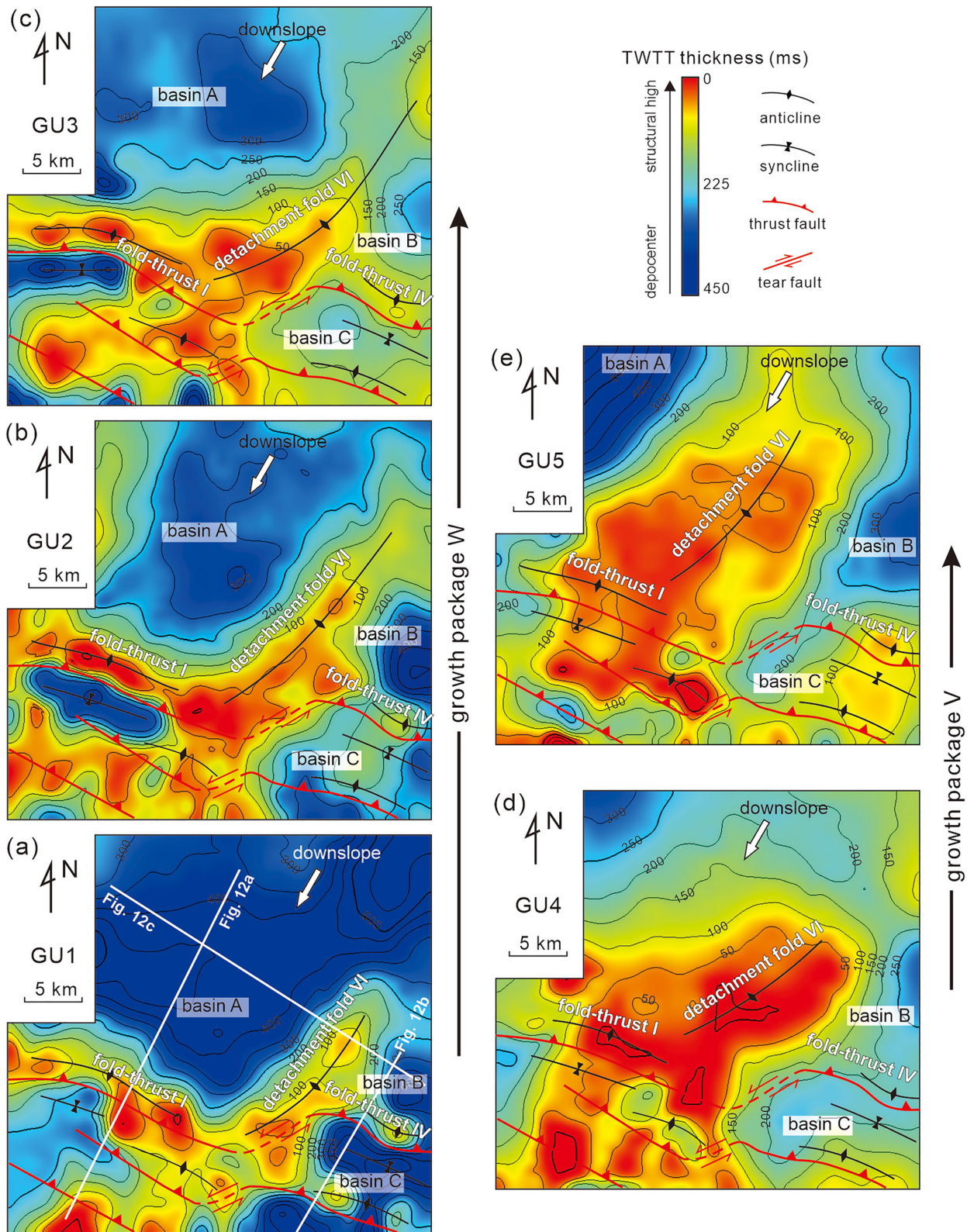


**Figure 13.** Isochron map for growth units within the growth package W (GU1–GU3) and V (GU4–GU5) showing the evolution of thrust-related structures and piggyback basins over the study area. The lower growth package W (GU1–GU3, a, b, c) features coevolution between thrusting and shale-detachment folding with piggyback basins well developed. The upper growth package V (GU4–GU5, d, e) is dominated by large shale-detachment fold with weakly active thrusting and limited piggyback basins. TWTT = two-way travel time.

crest in the western study area (Figure 12a), but well preserved at the lower-relief fold crest in the eastern study area (Figure 12b). Over the hanging walls of main thrusts, upward-shallowing of strata dips is poorly shown in growth package V indicating general low thrusting intensity. In contrast, upward-shallowing of strata dips in growth package V is apparent across the central detachment fold (Figure 12c), and the fold crest for each growth unit is mainly vertically stacked with less lateral migration. These suggest that the shale-detachment fold uplifted symmetrically and predominated over the weak thrust-related folding at time of growth package V.

Erosion-reconstructed isochron maps for GU4–GU5 (Figures 13d and 13e) reveal the dominance of oblique detachment fold that features broad fold crest occupying most of the central study area. The western fold-thrusts at this stage had largely merged with the central detachment fold, causing the western basin A to be limited to the northwestern side of the study area. The eastern basin B partly extends across the weakly active thrust faults. The elongated basin C between imbricate thrusts is poorly developed due to the lower thrusting intensity. At the time of GU4, the central detachment fold featured a broad gentle western limb and a narrow steep eastern limb (Figure 13d), which evolved to be symmetrical steep limbs with increased structural relief at the time of GU5 (Figure 13e). The basin A and B in GU5 expanded toward the central fold crest with onlap-thinning observed over the steep fold limbs (Figure 12c). These suggest that from GU4 to GU5 the central detachment fold had uplifted vertically, leading to the vertical stacking of growth units within the growth package V as opposed to the lateral migration of growth units within the growth package W (Figure 12c). Overall, analysis of the growth unit geometries and distributions demonstrates that the shale-detachment folding went through a transition from early lateral migration into late vertical uplift accompanied by the gradual weakening of thrusting.

### 5.3. Growth Package U (GU6–GU8): Weak Shale Detachment Folding

The upper growth package U is characterized by a set of high-amplitude, wavy-to-chaotic reflections involving extensive development of U-shaped to wedge-shaped channel-levee deposits (Figure 12). As the strata thins slightly toward the crest of fold-thrusts, several onlapping unconformities are observed along with local channel erosion, which define three component growth units (GU6–GU8). These growth units largely overlap the crest of fold-thrusts with rare upward-shallowing of dips, suggesting much lower growth rate of thrust faults with respect to the high sediment accumulation rate. Across the crest of the eastern fold-thrusts (Figure 12b), strata thickness changes minimally associated with a series of bypassed channel-levee deposits, suggesting much lower structural relief in the hanging wall that can hardly block the downslope transporting of sediment gravity flows. In contrast, the western fold-thrusts still kept some structural relief leading to the gradual thinning of growth units across the fold crest (Figure 12a). This structural relief diminished rapidly due to the high-rate infill of sediments within the associated basins and deep incision of channels over the structural highs. Across the central oblique detachment fold (Figure 12c), the wedge-shaped growth units show progressive decrease in dip upsection near the fold crest, with some of the crestal normal faults extending to the seafloor. These features reflect that the shale-detachment folding still continues until present day, but with a lower growth rate with respect to the high sediment accumulation rate.

Isochron maps for GU6–GU8 (Figures 14a, 14c, and 14e) reveal the progressive disappearance of the central detachment fold as the associated basins were filled up by deepwater sedimentary systems. With the thrusting being nearly stopped during this stage, the associated basins can extend beyond the main fold-thrusts showing elongated depocenters parallel to the regional slope. At time of GU6 (Figure 14a), the central detachment fold featured a narrow fold crest, while the western fold-thrusts still kept a structural relief. The topographic highs in the central-western study area separated the western confined basin A from the eastern unconfined basin B that extended beyond the eastern fold-thrusts. RMS amplitude map extracted within GU6 shows that highly sinuous aggradational channel complexes with widely extending levees bypassed the eastern elongated basin B (Figure 14b). Entering into GU7 (Figure 14c), the eastern basin B was almost filled up by the previous channel-levee deposits, leaving a nearly flat paleotopography at the eastern study area. Meanwhile, a deeply incised channel system in the western basin B broke through the topographic confinement, as shown in the corresponding seismic variance attribute map (Figure 14d), which cut out a narrow straight fairway over the crest of western fold-thrusts delivering sediments downslope (Figure 14c). During GU8 the basins were almost filled up leaving only a low-relief topographic remain of detachment

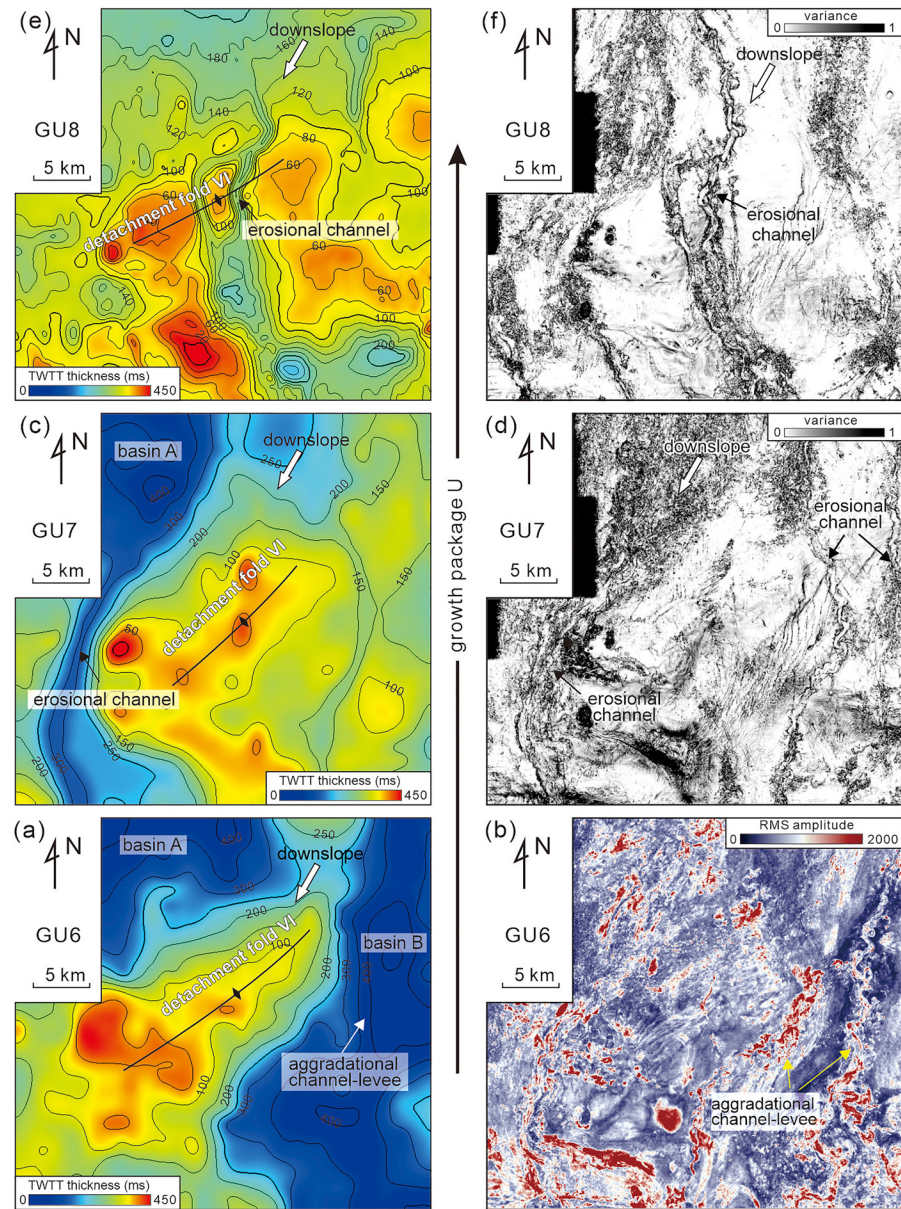


**Figure 14.** Isochron map for growth units within the youngest growth package U (GU6–GU8, a, c, e) and the corresponding seismic attribute map (b, d, f) showing the evolution of depocenters and deepwater sedimentary systems. The growth units feature elongated depocenters poorly confined by the weakly active structures. These depocenters are widely filled by submarine channel-levee systems. (b) is RMS amplitude map extracted within GU6 showing highly sinuous aggradational channel-levee bypassing the eastern basin B. (d) and (f) are seismic variance attribute extracted within GU7 and GU8 showing several moderate-sinuuous erosional channels crossing the structural highs. TWTT = two-way travel time.

fold in the central the study area (Figure 14e). Over this central topographic relief developed two narrow depocenters formed by smaller-scale erosional tributary channels that confluence downslope into a main channel, as shown in the corresponding seismic variance attribute map (Figure 14f). Overall, the elongated depocenters formed by channel bypassing swing from GU6 to GU8 without spatial inheritance, demonstrating that the central oblique detachment fold had much lower growth rate that was outpaced by the sediment accumulation rate, leading to the disappearance of thrust-related structures and associated basins on the modern seabed.

## 6. Discussion

### 6.1. 3D Shale Deformation Process Interacted With the Structural Evolution

As revealed by the structural distribution and evolution of growth units, the deepwater gravitational system consists of two sets of fold-thrusts laterally separated by an oblique shale-detachment fold. Deformation within the basal shale unit is believed to have played a fundamental role in controlling the evolution history of the shale-related structures. The shale-cored fold-thrusts in the western study area are the key structures that potentially record the role of shale deformation on the thrusting and folding deformation in the overburden. Similar fold-thrusts overlying thickened shale core have been previously documented in the literature (e.g., Maloney et al., 2010; Morley, 2009), but with different interpretations. One interpretation suggests that local shale thickening occurs preceding the development of break thrust that subsequently propagates downward to join the deeper detachment (Morley, 2009; Morley & Naghadeh, 2018; Morley et al., 2017). Another interpretation suggests that thickening within the basal shale unit occurs following the early phase of thrust-propagation folding (Maloney et al., 2010). Either interpretation, however, assumed that shale deformation was triggered by downslope gravitational contraction with shale shortening mainly occurring parallel to the regional slope, neglecting the role of lateral squeezing of shales that potentially results in more complex 3D shale deformation.

The 3D seismic interpretation in this study provides insight into the spatial morphology and deformation process of the basal shale unit, which helps to reinterpret the formation of shale-cored fold-thrusts from 3D perspective. The time structure map of the top prekinematic horizon (Figure 15b) reveals the proximity of the western shale-cored fold-thrusts to the central oblique detachment fold which was previously unnoted. Both structures are underlain by a large thickened shale core trending parallel to the regional slope, as shown in the isochron map of the Akata shales (Figure 15a). The thickness distribution of the basal shale unit is well correlated with the overlying structures (Figure 15b), suggesting an important connection between shale deformation and deformation styles in the overburden. As to the origin of this oblique shale core, there is a hypothesis that the shale may have a depocenter that was inverted to become the oblique trend, i.e., pre-tectonic shale thick. However, seismic section (Figure 10a) shows that the oblique shale core is primarily caused by shale thickening between marker reflections Y and Z, and spatially separates the eastern shale-thinning zone (averaging  $\sim 1,700$  ms in TWTT thickness) from the northwestern undeformed shale zone (averaging  $\sim 1,900$  ms in TWTT thickness). This feature suggests that the shale thick is closely related to redistribution of shales during the process of tectonic shortening, rather than a pre-tectonic, depositional shale thick. Considering the shortening of shales primarily occurs perpendicular to the regional slope, the downslope gravitational contraction is unlikely to be the direct cause for this oblique shale core. Based on the oblique orientation of shale core and thinning of shales in the eastern study area, we interpret that removed shales underneath the eastern fold-thrusts may have been laterally squeezed between marker reflections Y and Z resulting in northwestward shale thickening underneath the central detachment fold and western fold-thrusts. As this interpretation suggests, the marker reflection Z serves as the basal detachment level above which a horizontal slip lies. The overlap distance between reflections Y and Z is less than 20 km and is considered the greatest distance of lateral travel by thickened shales. This is feasible according to the analogs in nature or experiments that suggest the existence of tens of kilometers of contractional slip above the shale detachment (e.g., Butler & Paton, 2010; Dean et al., 2015).

Distribution of marker reflection Z provides more information on how lateral squeezing of shales may have progressed in space. Both marker reflection Z and the oceanic basement show a narrow NW-dipping slope zone in the southeastern margin of the study area (Figure 10a). According to the time structure map of the basement top (Figure 15d), the slope zone in the oceanic basement trends NE-SW and separates the southeastern zone of basement uplift from the central-northwestern zone of basement subsidence. This slope zone is likely caused by differential loading in response to redistribution of overlying shales. Marker reflection Z extends to the northwest subhorizontally and dies out near the undeformed shale zone (Figure 10a). A time slice at 6,250 ms crossing marker reflection Z shows the trace of the pinch-out points stretching out to the northwest in the central area (Figure 15c). Such pinch-out line represents the frontier of lateral shale squeezing where the horizontal slip along the basal detachment level Z stops. This suggests lateral shortening distance of shales varies along the strike of shale core between  $\sim 5$  and  $\sim 20$  km. The proposed model of lateral shale squeezing sufficiently explains the along-strike variations in shale deformation underlying the

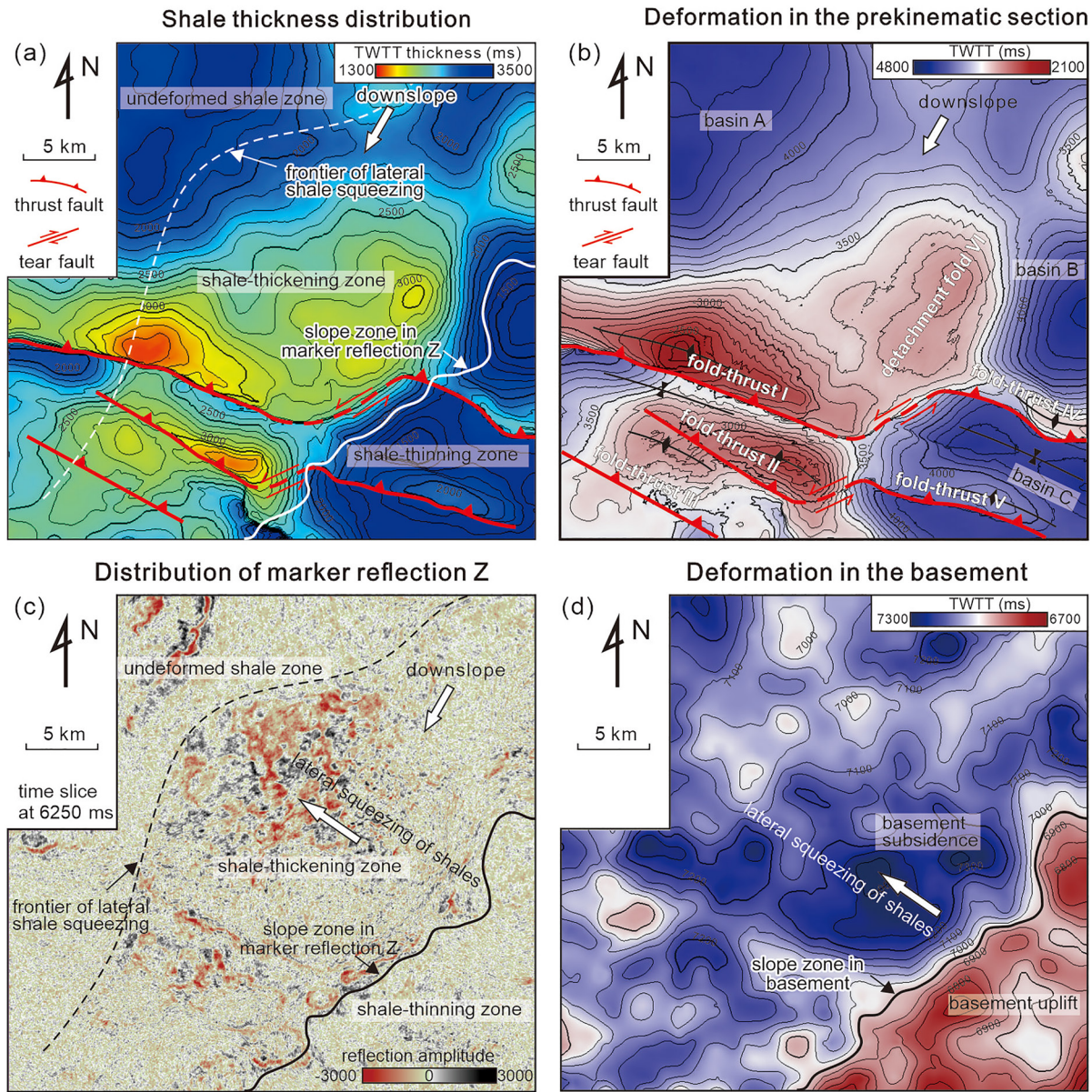


**Figure 15.** (a) Isochron map of the Akata Formation showing an oblique shale core underneath the central detachment fold and western fold-thrusts. The shale thickness underneath the eastern fold-thrusts is below regional average thickness of Akata shales. (b) Time structure map of the top prekinematic horizon showing deformation within the overburden comparable to that within the basal shale unit (a). (c) Seismic time slice at 6,250 ms showing northwest termination of marker reflection Z indicative of the frontier of lateral shale squeezing (dashed line). (d) Time structure map of the basement top showing NE-SW-trending structural slope in the basement (solid line). The frontier of lateral shale squeezing to the northwest and the structural slope to the southeast, confine the approximate extent of shale-thickening zone. TWTT = two-way travel time.

western fold-thrusts (Figures 8a–8c), and support the idea that the shale core underneath the western fold-thrusts originated from lateral squeezing of shale core underneath the adjacent central oblique detachment fold, not from downslope shortening of shales triggered by gravitational contraction.

Growth strata analysis and isochron maps of growth units suggest shale-detachment folding initiated in synchrony with downslope thrusting and folding in three dimensions, as opposed to two seemingly discrete processes in two dimensions (e.g., Maloney et al., 2010). The oblique shale-detachment fold initiated with a narrow crest and separated from the western fold-thrusts (GU1, Figure 13a). Thus early thrusting and folding in the western study area did not include shale thickening. Subsequently, the oblique shale-detachment fold migrated northwest and gradually merged with the western fold-thrusts (GU2–GU3, Figures 13b

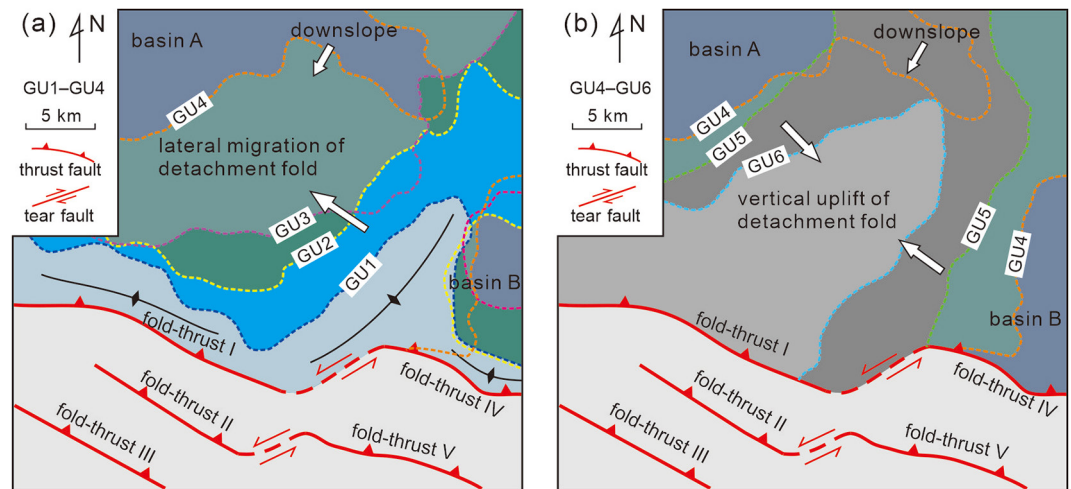


**Figure 16.** (a) Overlap map of 200 ms isochron contours from GU1 to GU4 showing early-stage lateral migration of the central oblique detachment fold. (b) Overlap map of 200 ms isochron contours from GU4 to GU6 showing late-stage vertical uplift of the central oblique detachment fold.

and 13c). As contours on the isochron maps approximate the positions of equal accommodation space related to similar topographic relief and slope, 200 ms isochron contours from each growth unit were selected to be overlain in map view (Figure 16), which reveals the continuous change of paleotopography in response to structural activity. Overlapping contour map from GU1 to GU4 (Figure 16a) shows early-stage lateral migration of the oblique detachment fold, resulting from the lateral movement of shales. Lateral squeezing of shales caused shale-cored fold-thrusts to gradually form in the western study area. The overlapping contour map from GU4 to GU6 (Figure 16b) shows the central oblique detachment fold transitioned from early-stage lateral migration to late-stage vertical uplift, with growth units vertically stacked in seismic profile (Figure 12c). This feature suggests deformation within the shale core was dominated by vertical thickening with minimal lateral movement of shales. The western fold-thrusts continued to uplift in response to the vertical thickening of shales, possibly corresponding to late-stage detachment folding as proposed by Maloney et al. (2010). Overall, spatiotemporal evolution of the growth units reveals synchronous timing of lateral shale squeezing with the main thrusting and folding as well as evidence that the shale deformation process involves an early-stage lateral movement and late-stage vertical thickening.

Regarding controlling factors behind the shale deformation process, this study proposes differential contraction between the western and eastern study areas may be a key factor influencing lateral movement of shales. As shown in Table 1, fold-thrust I in the western study area has much larger fold amplitude, fold wavelength, and fault displacement than fold-thrust IV in the eastern study area. This reflects the difference in structural shortening between these two adjacent fold-thrusts. The lateral differential structural shortening is considered to be largely consumed by the strike-slip tear fault linking fold-thrust I and IV (Figure 17a), and shear stress can be induced in the backlimb strata which may have promoted the oblique folding deformation (Figure 17b). Deep in the basal shale unit, the main thrusts terminate deeper in the western study area (below marker reflection Y) than in the eastern study area (below marker reflection X). With this lateral difference in thrust termination depth, the marker reflection Y uplifted in the western study area and gradually separated from its eastern counterpart, e.g., the marker reflection Z herein. As a consequence, the overpressure of shales beneath the western marker reflection Y was released generating east-to-west shale pressure difference, which may have driven the lateral movement of shales beneath marker reflection Y with the basal marker reflection Z detaching to the west. Figure 17b is a 3D block diagram illustrating how the lateral movement of shales may have interacted with the differential contraction in the overburden. This model remains to be substantiated by structural physical simulation experiments in the future. From the perspective of the wider Niger system, the variation of structural shortening in the localized study area is considered an effect of differential radial spreading of the delta higher on the slope (Figure 17a). During radial outward gravity spreading of the Niger Delta, the delta top extensional strain varied significantly along the strike of slope, leading to extensive development of delta toe oblique extensional tear faults and

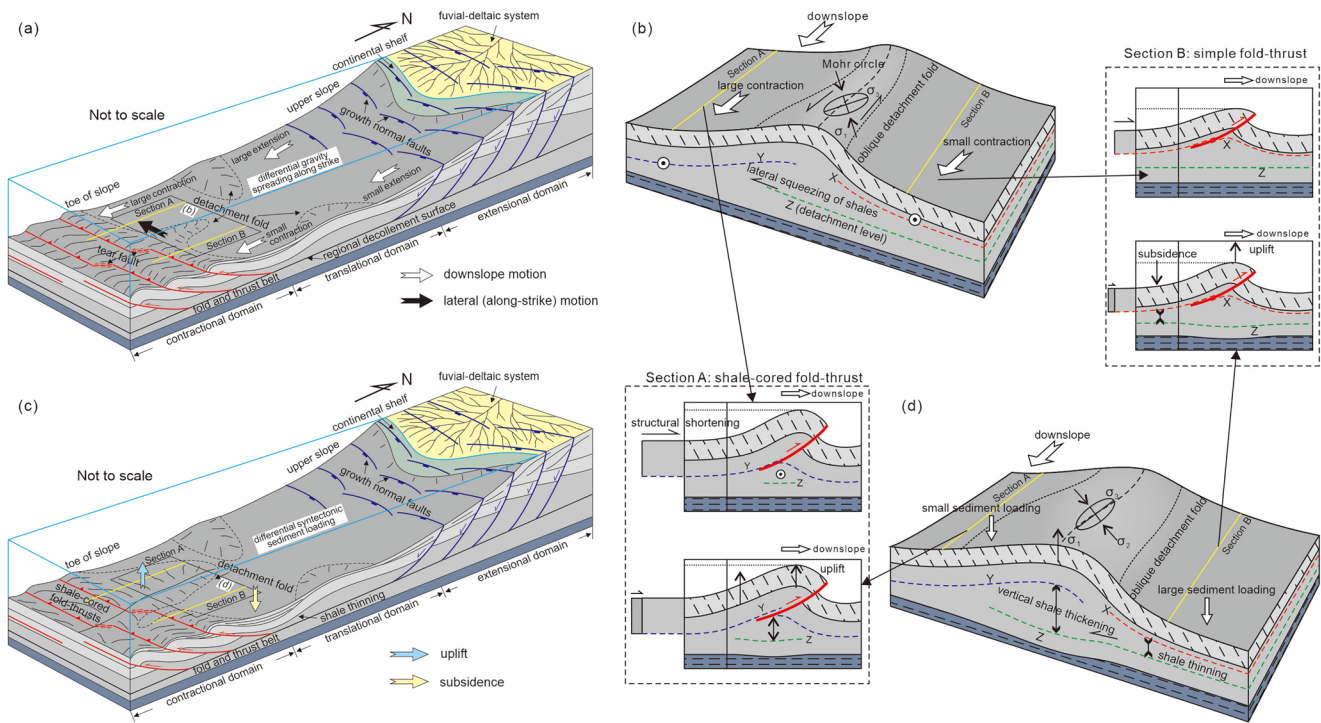


**Figure 17.** Schematic illustration of 3D shale deformation interacted with downslope thrusting. (a) Regional 3D cartoon showing the spatial configuration between down-dip thrust-related structures and up-dip extensional structures. Differential gravity spreading along the strike of continental slope is the main driver for the development of oblique tear faults and detachment folds. The lateral and downslope motions are indicated by black and white arrows, respectively. (b) Early-stage lateral shale squeezing induced by differential contraction. During this stage the central oblique detachment fold initiated and migrated laterally, while the shale-cored fold-thrusts gradually formed. (c) Regional 3D cartoon showing the evolution of delta toe oblique structures in response to differential syntectonic sediment loading. The oblique detachment fold uplifted (cyan arrow) with a broad fold crest, while the adjacent synclines subsided (yellow arrow) with thick syntectonic sediments deposited. (d) Late-stage vertical shale thickening caused by differential loading from syntectonic sediments. The overburden continued to uplift despite the weak thrusting during this stage. Section A illustrates the evolution of shale-cored fold-thrusts and section B illustrates the evolution of simple fold-thrusts.

segmented thrusts (Figure 1a, after Wu et al. [2015]). The differential spreading of deltas is a common feature of large fluvial-deltaic systems, such as the Orange system offshore Namibia, the Amazon system offshore Brazil, and the Baram system offshore Brunei, where similar delta toe oblique structures have been recognized (e.g., Morley, 2009; Morley et al., 2011; Scarselli et al., 2016; Yang et al., 2020). This study, despite the limited area, documents a delta toe oblique structure style potentially representative of other parts of the Niger system with differential gravity spreading along strike and down-dip transition between translational zone (shale deformation zone) and fold-thrust belt (Figure 17a). The mechanism proposed in this study reveals the relationship between oblique structures and shale deformation (Figure 17b), which has not been fully evaluated from early studies and may be applied to other oblique structures in the Niger system or within similar systems elsewhere.

Differential sediment loading is another important factor potentially contributing to lateral squeezing of shales. Previous studies revealed that overpressured shales, at times similar to mobile salt units, can deform in response to differential sediment loading and produce a series of shale-withdrawal minibasins (Blanchard et al., 2019; Dean et al., 2015; Duerto & McClay, 2011; Galindo & Lonergan, 2020; Ings & Beaumont, 2010; Ruh et al., 2018; Soto et al., 2010). The differential sediment loading here is considered to mainly arise from syntectonic sediment loading, since pre-tectonic sediment loading changes minimally across the study area with nearly isopachous strata (Figure 17c). In this study, we attribute the differential sediment loading between western and eastern study areas to asymmetrical migration of growth units, especially during growth package W. With the gradual uplifting of the western limb of the central detachment fold, the depocenters of overlying growth units (GU1–GU3) migrated northwest, contrasting with the eastern limb over which the growth unit depocenters were almost stacked vertically (Figure 16a). Consequently, the larger sediment

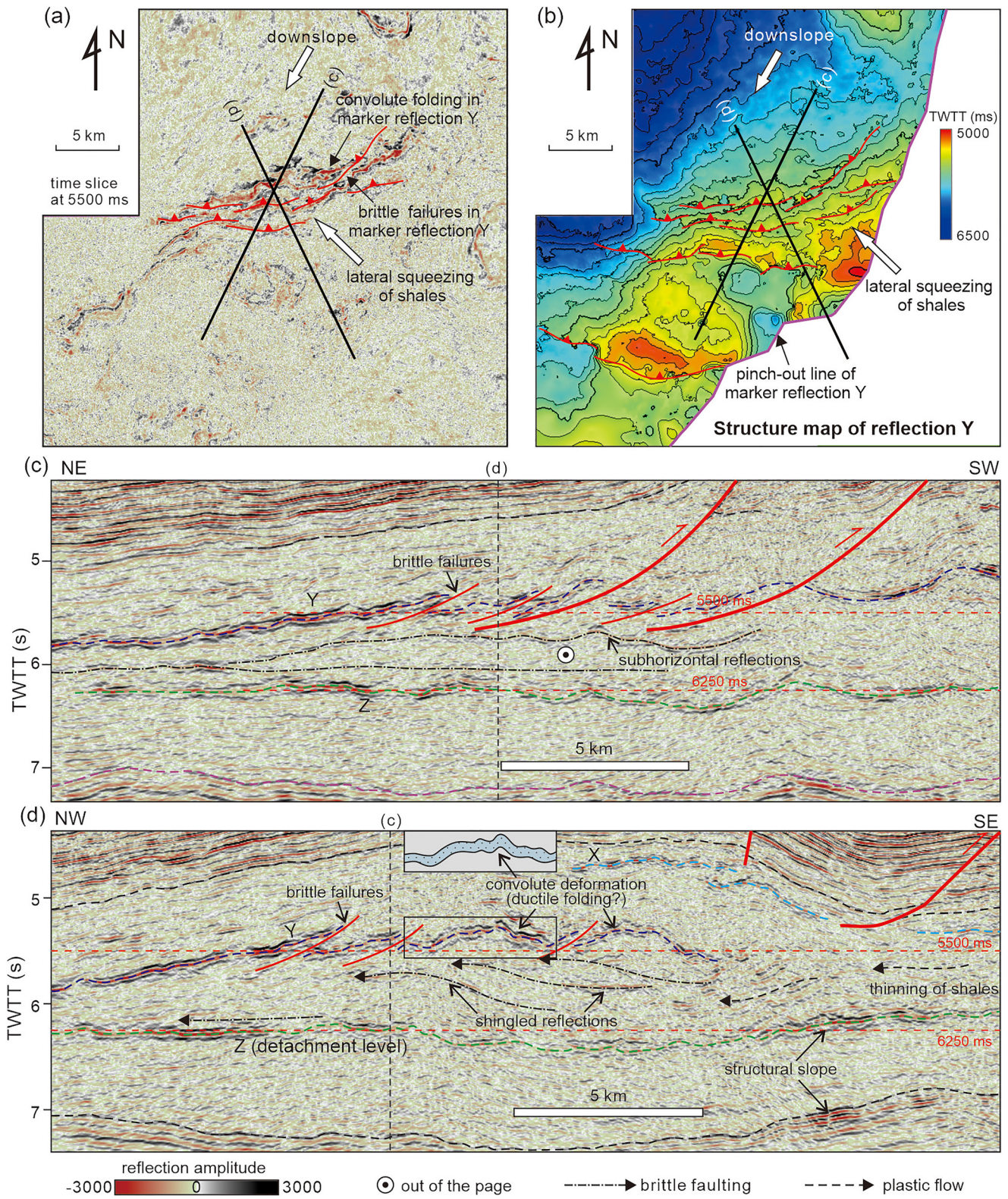


loading in the eastern study area could cause evacuation of shales within the basal shale unit and the removed shales would be squeezed into the adjacent fold core which was overlaid with smaller sediment loading (Figures 17c and 17d). The effects of differential sediment loading could dominate those of differential contraction as thrusting intensity weakened greatly following growth package W. Accordingly, deformation within the basal shale unit was dominated by vertical shale thickening with minor lateral movement of shales, which resulted in the vertical uplift of the detachment fold. Local extension was generated over the crest of uplifting detachment fold with two sets of crestal normal faults cutting through the overburden (Figure 10). The shale-detachment folding gradually weakened with the decreased differential sediment loading over time. Figure 17d illustrates how the vertical thickening of shales interacted with the differential sediment loading from growth strata. This model reflects potential shale tectonic features discussed in the following section.

## 6.2. Deformation Mechanisms Within the Basal Shale Unit

External factors including differential contraction and differential loading, have been discussed to exert significant controls on the shale deformation process, which is crucial to the structural evolution over the study area. The deformation mechanisms within the basal shale unit, however, are still a subject of controversy and poorly constrained in lack of sufficient evidence from high-quality seismic data. Traditionally, ductile deformation is believed to be fundamental in the shale deformation process. The term “mobile shale” was commonly used to illustrate the plastic flow occurring in the seismic-unresolved unit (e.g., Briggs et al., 2006; Cohen & McClay, 1996; Latta & Anastasio, 2007; Morley, 2003; Morley & Guerin, 1996; Wiener et al., 2010). Improved quality of seismic reflection data has prompted more recent work on the reinterpretation of mobile shale which has largely been imaged as incoherent reflectivity, and structural thickening through brittle deformation has been suggested to play an important role in accommodating strain within a basal shale unit (e.g., Couzens-Schultz et al., 2003; Maloney et al., 2010; Morgan, 2015; Morley et al., 2017, 2011; Plesch et al., 2007). By providing more details of seismic reflection within the deformed shale unit, this study demonstrates that brittle and ductile deformations are combined in the shale deformation process, as previously suggested (e.g., Duerto & McClay, 2011; Maloney et al., 2010; Morley et al., 2017, 2018, 2011; Van Rensbergen & Morley, 2003), via a series of multiscale brittle failures and plastic flows. Although it is well known that the subseismic deformation such as lateral compaction can be a major element in poorly consolidated sequences (e.g., Butler & Paton, 2010), our main concern in this study is seismic-observed deformation within the weak shale units that ranges from hundreds to thousands of meters in scale.

Brittle deformation is proven to have occurred within the basal shale unit at various scales effectively transferring horizontal displacement into vertical thickening of the shale unit. We define the levels of brittle failures based on the relative scale and configuration relationship between brittle surfaces. (1) The marker reflection Z beneath the shale core is defined as the first level of brittle failure surface, which served as the master detachment level with significant horizontal slip above. New brittle failures gradually formed in the frontier of reflection Z as it extended to the northwest during the lateral squeezing of shales (Figure 18d). This brittle extension of the master detachment allows horizontal shortening of shales to continue at the base which was then transferred into vertical thickening of shales. (2) The marker reflection Y on top of the shale core exhibits discontinuous segments displaced by a series of secondary thrust faults (Figures 18c and 18d), and these faults are defined as the second level of brittle failures contributing to local thickening on top of the shale core. As shown on the time slice at 5,500 ms (Figure 18a) and the time structure map of reflection Y (Figure 18b), these secondary thrust faults trend oblique to the regional slope and likely formed due to the combined effect of downslope contraction and lateral squeezing of shales. (3) Within the thickened shale core, several shingled, moderate-amplitude trough reflectors are visible in the strike-oriented reflection profile (Figure 18d), which are subhorizontal in the strike-normal reflection profile (Figure 18d). These shingled reflections are defined as the third level of brittle failures forming an oblique thrust duplex structure within the shale core. This kind of thrust duplex structure is considered a key element in transferring horizontal shortening into vertical thickening of the shale unit. Besides, the subseismic scale of brittle failures is also expected to contribute to the thickening shale core. Similar thrust duplex (Morley et al., 2017; Plesch et al., 2007) or anticlinal stack (Maloney et al., 2010; Noack, 1995) through multiscale brittle failures are reported in the literature, which suggest that brittle deformation occurring at multiple



scales can cause rapid growth of the detachment fold with relatively little displacement while also being able to accommodate strain within the detachment-fold core without plastic flow (Maloney et al., 2010).

A lack of thinned regions of Akata shale in adjacent areas is recognized as an important clue which supports structural thickening through brittle deformation instead of mobile shale flowing into the anticlinal core (Maloney et al., 2010). In this study, however, thinning shales adjacent to the thickened shale core are observed in the eastern study area (Figure 15a). The prekinematic Agbada Formation overlying the thinned eastern region of Akata shale exhibits apparent synclinal geometry with a group of growth units continuously filling the depocenters and onlapping to adjacent fold limbs (Figures 4a and 12c). These features are similar to the Bahia basin offshore Colombian Caribbean (Galindo & Lonergan, 2020), which are believed to indicate downbuilding trend of the syncline and represent shale tectonic features. Thus, it is interpreted that ductile shale had withdrawn beneath the eastern study area and flowed into the adjacent detachment-fold core, contributing to the growth of detachment fold (Figure 19a). As a result, the eastern basin B may have transitioned from an early piggyback style basin into a shale-withdrawal minibasin (Figure 19a), but as the basin is not fully covered by the seismic data set, it is unclear whether it is indeed a subcircular or oval basin. However, a closer look at the elongated basin C finds a smaller subcircular depression (Figures 19a and 19b), which occurred during GU3–GU5 (Figure 19c). This feature can support the interpretation of shale tectonics to some degree. In addition to the local flow of shales from beneath synclines adjacent to the fold core, the marker reflection Y on top of the thickened shale core is deformed with convolute geometries, as shown on the reflection profile and time slice (Figures 18a, 18c, and 18d). These kinds of convolute deformations are related to secondary thrust faults in the shales and are a likely indication of ductile folding deformation in the process of shale thickening. Since what appears to be ductile on seismic could be brittle at outcrop or well scale, there remains a need to test the seismic interpretation of ductile shale deformation when additional well data become available. Despite this seismic uncertainty, ductile deformation combined with multiscale brittle failures has been suggested to effectively fill the void created by fold amplification (e.g., Maloney et al., 2010; Morley et al., 2017; Van Rensbergen & Morley, 2003). Overall, much of the evidence from this study supports the recent view that most of what was previously assumed to be chaotic shale “diapirs” are actually shale-cored anticlinal folds with complex internal structures of faulting and folding (e.g., Duerto & McClay, 2011; Maloney et al., 2010; Morley et al., 2017), and also emphasizes that the local flow of shales characteristic of mobile shales can occur beneath adjacent synclines.

Seismic imaging of the shale internal structures suggests that lateral squeezing of shales from syncline regions into adjacent fold cores occurred through a mixture of local flow of shales, ductile folding, and multiscale fault structures (basal detachment level, top thrust faults, and internal thrust duplex) as summarized in Figure 20. The local flow of shales observed in the eastern study area reflects the nature of mobile shales, while the incoherent structures within the shale core more reflect the nature of brittle shales. A similar mixture of brittle shales and softer mudrocks has also been interpreted in the Cenozoic Eastern Venezuelan fold and thrust belt based on clear seismic imaging and drilling cores (Duerto & McClay, 2011). As a matter of fact, a strict distinction between ductile and brittle deformations is difficult to make for shales because the pressure-temperature conditions would change during burial and cause evolution of shale properties. It is assumed that the change of shale composition and pore-fluid pressure allows plastic flow in water-rich mudrocks to transition into brittle deformation in stiffer shales as temperatures reach around 80°C at a depth of >2–3 km (Day-Stirrat et al., 2010; Thyberg et al., 2010), the resulting deformation of both viewed macroscopically may look ductile and may involve squeezing of shales from areas of high pore-fluid pressure to areas of lower pore-fluid pressure. Due to improved seismic resolution and new understanding of chemical diagenesis in shales, the existence of thick, deeply buried mobile shales has been widely challenged (e.g., Day-Stirrat et al., 2010; Duerto & McClay, 2011; Morley et al., 2017, 2018; Van Rensbergen & Morley, 2003). Nonetheless, other strong cases are found in the Bahia basin offshore Colombian Caribbean (Galindo & Lonergan, 2020), the Shannon basin offshore Ireland (Blanchard et al., 2019), the Alboran Sea (Western Mediterranean) (Soto et al., 2010), and other parts of the deepwater Niger Delta

**Figure 18.** Seismic reflection characteristics within the basal shale unit showing the shale deformation mechanisms. Seismic time slice at 5,500 ms (a) and time structure map of marker reflection Y (b) show the map view of several brittle failures and ductile folding in marker reflection Y. Sections (c) and (d) are inset maps from Figures 8a and 10b, respectively, showing both brittle and ductile deformations within the basal shale unit. Several shingled moderate-amplitude reflections are recognized within the shale core forming a thrust duplex structure (d), which are subhorizontal in section (c). Plastic flow occurring near the shale-thinning zone also contributes to the thickening of detachment-fold interior. TWTT = two-way travel time.

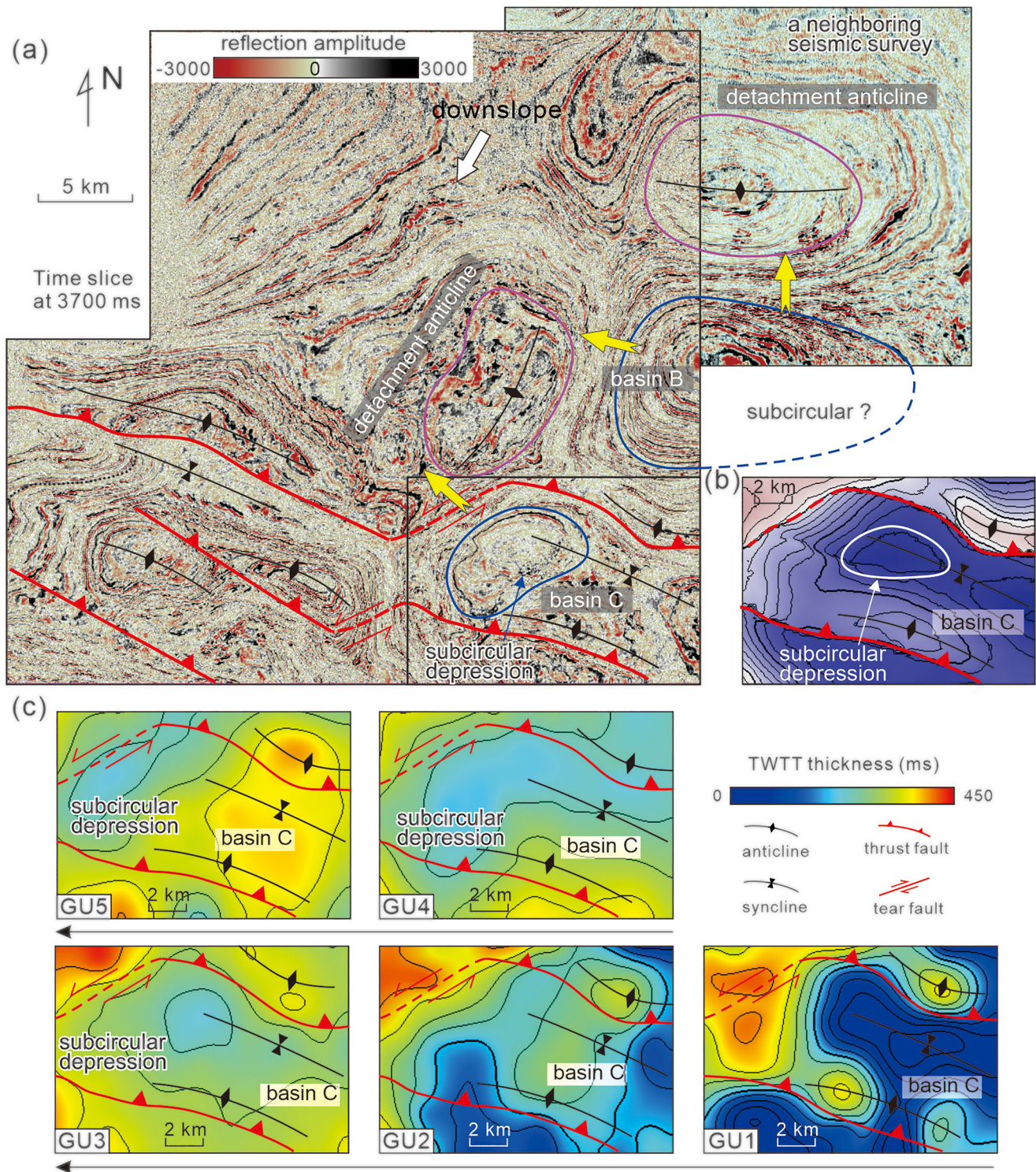


**Figure 19.** Seismic time slice at 3,700 ms (a) and inset maps from the time structure map of the top prekinematic horizon (b) and isochron maps of GU1–GU5 (c), showing shale tectonic features. The yellow arrows indicate local flow of shales from beneath synclines into adjacent anticline cores. The subcircular morphology of basin B has yet to be tested in the absence of seismic data southeast of the study area. The elongated basin C contains a smaller subcircular depression which occurred during GU3–GU5.

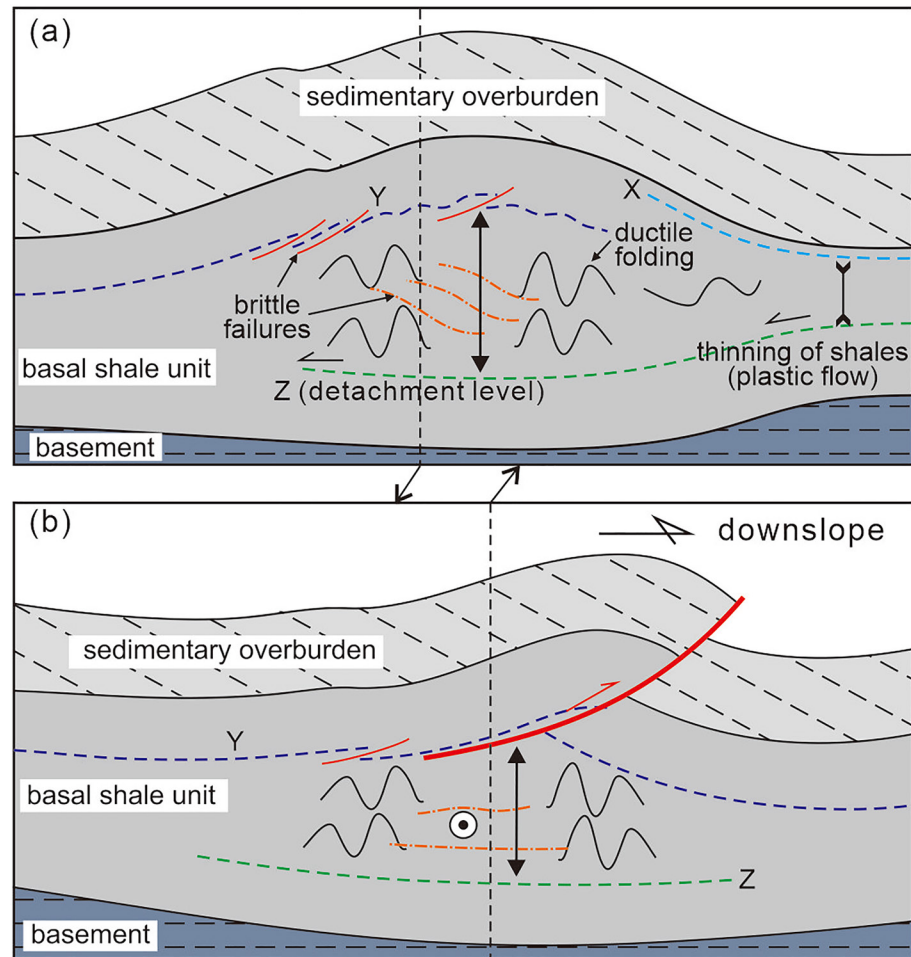


**Figure 20.** Schematic illustration of shale deformation mechanisms. (a) Cross section of detachment-fold core showing the combination of multiscale brittle failures, ductile folding and local plastic flow of shales. (b) Cross section of shale-cored fold-thrusts showing the deformation features associated with lateral squeezing of shales.

(e.g., Krueger & Grant, 2011; Morley & Guerin, 1996; Wiener et al., 2010), where evidence such as the downbuilding synformal depocenters and the development of shale-withdrawal minibasins lends support to the mobile shale interpretation. Quantitative evaluation of gravity-driven deformation from the Orange Basin offshore Namibia also reveals that subseismic ductile deformation, likely as lateral compaction and volume loss, can be necessary to balance the mismatch between contractional strain and extension higher on the slope (Butler & Paton, 2010). A numerical model from Dean et al. (2015) suggests that oceanward thinning of the Akata shales in the Niger Delta prompted deformation in mobile shale to occur further oceanward, thus enabling the development of a second outer fold and thrust belt separated from the first by a largely undeformed zone. This may explain the local presence of mobile shales in the study area lying between the outer fold and thrust belt and translational zone. Overall, this study complements recent work on reinterpretation of mobile shale substantiating the claim that unlike salt deformation, shale deformation can involve more complex (both ductile and brittle) mechanisms and have more individualized variability in thickness, structure, and macroscopic deformation style within basal shale units. As previously suggested (e.g., Morley et al., 2017, 2018), this variability is the result of multiple factors that interconnected on several scales, such as mechanical stratigraphy, pore-fluid pressure, shale mineralogy, deformation rate, and pressure-temperature conditions.

## 7. Conclusions

This study provides an example of a deepwater gravitational system developed above a deformed shale unit, improving our understanding of the role of shale deformation in a gravity-driven setting. The studied deepwater gravitational system consists of three structural styles: shale-cored fold-thrusts, fold-thrusts without shale core, and oblique detachment fold. All three structural styles are spatially connected and coevolved through time as related to redistribution of the underlying shales. Based on the oblique orientation of detachment fold and 3D deformation within the basal shale unit, we conclude that the oblique shale core beneath the fold crest was formed by lateral squeezing of shales beneath adjacent synclines, rather than due to downslope contraction. The differential contraction between adjacent fold-thrusts is considered a key factor in controlling lateral movement of shales, which had been dominated by vertical thickening of shales as a result of differential loading from asymmetrically stacked growth units overwhelmed the weakened thrusting. Seismic imaging of the shale internal structures also confirms that redistribution of shales occurred through combined ductile and brittle deformations (instead of any single mechanism), involving local flow of shales, ductile folding, and multiscale fault structures. This conclusion complements recent work reinterpreting mobile shale, emphasizing the continued existence of mobile shale locally (mostly beneath the synclines) despite the general reinterpretation of thickened shales within the detachment-fold core as complex internal structures of faulting and folding (not salt-like shale “diapirs”). This study highlights the fundamental role that shale deformation may play on the various structural styles (particularly the oblique folds and faults) in a gravity-driven setting and supports previous understanding that shale deformation behaviors show great complexity and variability as caused by multiple factors at a variety of scales.

## Data Availability Statement

We thank the China National Offshore Oil Corporation for providing and permitting publication of the subsurface data. We would like to thank our colleagues, Zihao Liu, Mei Chen, Zhao Liu, and Shuaibo Zhang for their help with seismic data interpretation and data analysis. We deeply thank *Tectonics* Editor Laurent Jolivet, Prof. Chris Morley from the Chiang Mai University, Prof. Lidia Lonergon from the Imperial College London, Prof. Lisa McNeill from the University of Southampton, Dr. Xiaodong Yang from the Institut de Physique du Globe de Paris, and an anonymous reviewer for their constructive comments that considerably strengthened, clarified, and broadened the impact of this text. The seismic reflection profile data used in this study are available from <https://doi.org/10.6084/m9.figshare.12057048.v3>.

## Acknowledgments

This study was funded by the National Planned Major Science and Technology Projects of China (No. 2011ZX05030-005-02), the National Natural Science Foundation of China (No. 41772101), and the Strategic Cooperation Technology Projects of CNPC and CUPB (No. ZLZX2020-02). Zhang is supported by the National Natural Science Foundation of China (No. 42002112), the China Postdoctoral Science Foundation (No. 2020M670580), as well as the Science Foundation of China University of Petroleum-Beijing (No. 2462020XKBH008). Special thanks go to Natasha Thomas from the University of Texas at Austin for her help on the language editing.

## References

- Ajakaiye, D. E. & Bally, A. W. (2002). Some structural styles on reflection profiles from offshore Niger Delta. *Search and Discovery*, 10031, 1–6.
- Avbovo, A. A. (1978). Tertiary lithostratigraphy of Niger Delta. *American Association of Petroleum Geologists Bulletin*, 62, 295–306.
- Benesch, N. P., Plesch, A., & Shaw, J. H. (2014). Geometry, kinematics, and displacement characteristics of tear-fault systems: An example from the deep-water Niger Delta. *American Association of Petroleum Geologists Bulletin*, 98, 465–482. <https://doi.org/10.1306/06251311013>
- Bergen, K. J., & Shaw, J. H. (2010). Displacement profiles and displacement-length scaling relationships of thrust faults constrained by seismic-reflection data. *Geological Society of America Bulletin*, 122, 1209–1219. <https://doi.org/10.1130/b26373.1>
- Bilotti, F., & Shaw, J. H. (2005). Deep-water Niger Delta fold and thrust belt modeled as a critical-taper wedge: The influence of elevated basal fluid pressure on structural styles. *American Association of Petroleum Geologists Bulletin*, 89, 1475–1491. <https://doi.org/10.1306/06130505002>
- Blanchard, S., Matheson, E. J., Fielding, C. R., Best, J. L., Bryk, A. B., Howell, K. J., et al. (2019). Early burial mud diapirism and its impact on stratigraphic architecture in the Carboniferous of the Shannon Basin, County Clare, Ireland. *Sedimentology*, 66(1), 329–361. <https://doi.org/10.1111/sed.12492>
- Bonini, M. (2003). Detachment folding, fold amplification, and diapirism in thrust wedge experiments. *Tectonics*, 22, 1065. <https://doi.org/10.1029/2002TC001458>
- Briggs, S. E., Davies, R. J., Cartwright, J. A., & Morgan, R. (2006). Multiple detachment levels and their control on fold styles in the compressional domain of the deepwater west Niger Delta. *Basin Research*, 18, 435–450. <https://doi.org/10.1111/j.1365-2117.2006.00300.x>
- Brun, J.-P., & Fort, X. (2004). Compressional salt tectonics (Angolan margin). *Tectonophysics*, 382, 129–150. <https://doi.org/10.1016/j.tecto.2003.11.014>
- Burbank, D., Meigs, A., & Brozović, N. (1996). Interactions of growing folds and coeval depositional systems. *Basin Research*, 8, 199–223. <https://doi.org/10.1046/j.1365-2117.1996.00181.x>
- Burbank, D. W., & Verges, N. (1994). Reconstruction of topography and related depositional systems during active thrusting. *Journal of Geophysical Research*, 99, 281–297. <https://doi.org/10.1029/94JB00463>
- Butler, R. W. H., & Paton, D. A. (2010). Evaluating lateral compaction in deepwater fold and thrust belts: How much are we missing from “nature’s sandbox”? *Geological Society of America Today*, 20(3), 4–10. <https://doi.org/10.1130/gsatg77a.1>

- Clark, I. R., & Cartwright, J. A. (2009). Interactions between submarine channel systems and deformation in deepwater fold belts: Examples from the Levant Basin, Eastern Mediterranean Sea. *Marine and Petroleum Geology*, 26, 1465–1482. <https://doi.org/10.1016/j.marpetgeo.2009.05.004>
- Clark, I. R., & Cartwright, J. A. (2011). Key controls on submarine channel development in structurally active settings. *Marine and Petroleum Geology*, 28, 1333–1349. <https://doi.org/10.1016/j.marpetgeo.2011.02.001>
- Clark, I. R., & Cartwright, J. A. (2012). Interactions between coeval sedimentation and deformation from the Niger Delta deepwater fold belt. *Society for Sedimentary Geology Special Publication*, 99, 243–267. <https://doi.org/10.2110/pec.12.99.0243>
- Cohen, H. A., & McClay, K. (1996). Sedimentation and shale tectonics of the northwestern Niger Delta front. *Marine and Petroleum Geology*, 13, 313–328. [https://doi.org/10.1016/0264-8172\(95\)00067-4](https://doi.org/10.1016/0264-8172(95)00067-4)
- Corredor, F., Shaw, J. H., & Bilotti, F. (2005). Structural styles in the deep-water fold and thrust belts of the Niger Delta. *American Association of Petroleum Geologists Bulletin*, 89, 753–780. <https://doi.org/10.1306/02170504074>
- Couzens-Schultz, B. A., Vendeville, B. C., & Wiltschko, D. V. (2003). Duplex style and triangle zone formation: Insights from physical modeling. *Journal of Structural Geology*, 25, 1623–1644. [https://doi.org/10.1016/s0191-8141\(03\)00004-x](https://doi.org/10.1016/s0191-8141(03)00004-x)
- Curry, M. A. E., Peel, F. J., Hudec, M. R., & Norton, I. O. (2018). Extensional models for the development of passive-margin salt basins, with application to the Gulf of Mexico. *Basin Research*, 30, 1180–1199. <https://doi.org/10.1111/bre.12299>
- Damuth, J. E. (1994). Neogene gravity tectonics and depositional processes on the deep Niger Delta continental margin. *Marine and Petroleum Geology*, 11, 320–346. [https://doi.org/10.1016/0264-8172\(94\)90053-1](https://doi.org/10.1016/0264-8172(94)90053-1)
- Day-Stirrat, R. J., McDonnell, A., & Wood, L. J. (2010). Diagenetic and seismic concerns associated with interpretation of deeply buried “mobile shales”. In L. Wood (Ed.), *Shale tectonics* (Vol. 93, pp. 5–27). American Association of Petroleum Geologists Memoir.
- Dean, S., Morgan, J., Brandenburg, J. P., Wang, D., Li, J., Cheng, P., et al. (2015). Influence of mobile shale on thrust faults: Insights from discrete element simulations. *American Association of Petroleum Geologists Bulletin*, 99, 403–432. <https://doi.org/10.1306/10081414003>
- Deville, E., Guerlais, S.-H., Callec, Y., Griboulard, R., Huyghe, P., Lallemand, S., et al. (2006). Liquefied vs stratified sediment mobilization processes: Insight from the South of the Barbados accretionary prism. *Tectonophysics*, 428, 33–47. <https://doi.org/10.1016/j.tecto.2006.08.011>
- Doust, H., & Omatsola, E. (1990). Niger Delta. In J. O. Edwards, & P. A. Santogross (Eds.), *Divergent passive margin basins Tulsa* (Vol. 48, pp. 201–238). American Association of Petroleum Geologists Memoir.
- Duerto, L., & McClay, K. (2011). Role of the shale tectonics on the evolution of the Eastern Venezuelan Cenozoic thrust and fold belt. *Marine and Petroleum Geology*, 28, 81–108. <https://doi.org/10.1016/j.marpetgeo.2009.11.005>
- Epard, J.-L., & Groshong, R. H. (1995). Kinematic model of detachment folding including limb rotation, fixed hinges and layer-parallel strain. *Tectonophysics*, 247, 85–103. [https://doi.org/10.1016/0040-1951\(94\)00266-c](https://doi.org/10.1016/0040-1951(94)00266-c)
- Fadiya, L. S., & Salami, B. M. (2015). A Neogene calcareous nannofossil biozonation scheme for the deep offshore Niger Delta. *Journal of African Earth Sciences*, 112, 251–275. <https://doi.org/10.1016/j.jafrearsci.2015.08.018>
- Fillon, C., Huisman, R. S., van der Beek, P., & Muñoz, J. A. (2013). Syntectonic sedimentation controls on the evolution of the southern Pyrenean fold-and-thrust belt: Inferences from coupled tectonic-surface processes models. *Journal of Geophysical Research: Solid Earth*, 118, 5665–5680. <https://doi.org/10.1002/jgrb.50368>
- Galindo, P. A., & Lonergan, L. (2020). Basin evolution and shale tectonics on an obliquely convergent margin: The Bahia basin, offshore Colombian Caribbean. *Tectonics*, 39, e2019TC005787. <https://doi.org/10.1029/2019TC005787>
- Gao, B., Flemings, P. B., Nikolinakou, M. A., Saffer, D. M., & Heidari, M. (2018). Mechanics of fold-and-thrust belts based on geomechanical modeling. *Journal of Geophysical Research: Solid Earth*, 123, 4454–4474. <https://doi.org/10.1029/2018JB015434>
- Gee, M. J. R., & Gawthorpe, R. L. (2006). Submarine channels controlled by salt tectonics: Examples from 3D seismic data offshore Angola. *Marine and Petroleum Geology*, 23, 443–458. <https://doi.org/10.1016/j.marpetgeo.2006.01.002>
- Giles, K. A., & Rowan, M. G. (2012). Concepts in halokinetic-sequence deformation and stratigraphy. *Geological Society, London, Special Publications*, 363, 7–31. <https://doi.org/10.1144/sp363.2>
- Gong, C., Wang, Y., Hodgson, D. M., Zhu, W., Li, W., Xu, Q., & Li, D. (2014). Origin and anatomy of two different types of mass-transport complexes: A 3D seismic case study from the northern South China Sea margin. *Marine and Petroleum Geology*, 54, 198–215. <https://doi.org/10.1016/j.marpetgeo.2014.03.006>
- Hansberry, R. L., King, R., Collins, A. S., & Morley, C. K. (2014). Complex structure of an upper-level shale detachment zone: Khao Khwang fold and thrust belt, Central Thailand. *Journal of Structural Geology*, 67, 140–153. <https://doi.org/10.1016/j.jsg.2014.07.016>
- Heiniö, P., Davies, R. J., Yang, J., Song, P., He, W., Howlett, D. M., et al. (2006). Degradation of compressional fold belts: Deep-water Niger Delta. *American Association of Petroleum Geologists Bulletin*, 90, 753–770. <https://doi.org/10.1306/11210505090>
- Henriksen, S., Helland-Hansen, W., & Bullimore, S. (2011). Relationships between shelf-edge trajectories and sediment dispersal along depositional dip and strike: A different approach to sequence stratigraphy. *Basin Research*, 23, 3–21. <https://doi.org/10.1111/j.1365-2117.2010.00463.x>
- Higgins, S., Clarke, B., Davies, R. J., & Cartwright, J. (2009). Internal geometry and growth history of a thrust-related anticline in a deep water fold belt. *Journal of Structural Geology*, 31, 1597–1611. <https://doi.org/10.1016/j.jsg.2009.07.006>
- Higgins, S., Davies, R. J., & Clarke, B. (2007). Antithetic fault linkages in a deep water fold and thrust belt. *Journal of Structural Geology*, 29, 1900–1914. <https://doi.org/10.1016/j.jsg.2007.09.004>
- Hudec, M. R., Jackson, M. P. A., & Schultz-Ela, D. D. (2009). The paradox of minibasin subsidence into salt: Clues to the evolution of crustal basins. *Geological Society of America Bulletin*, 121, 201–221.
- Huyghe, P., Foata, M., Deville, E., Mascle, G., & Group, C. W. (2004). Channel profiles through the active thrust front of the southern Barbados prism. *Geological Society of America Bulletin*, 32, 429–432. <https://doi.org/10.1130/g20000.1>
- Ings, S. J., & Beaumont, C. (2010). Continental margin shale tectonics: Preliminary results from coupled fluid-mechanical models of large-scale delta instability. *Journal of the Geological Society*, 167(3), 571–582. <https://doi.org/10.1144/0016-76492009-052>
- Jackson, M. P. A., & Talbot, C. J. (1986). External shapes, strain rates, and dynamics of salt structures. *Geological Society of America Bulletin*, 97, 305–323. [https://doi.org/10.1130/0016-7606\(1986\)97<305:essrad>2.0.co;2](https://doi.org/10.1130/0016-7606(1986)97<305:essrad>2.0.co;2)
- Jamison, W. R. (1987). Geometric analysis of fold development in overthrust terranes. *Journal of Structural Geology*, 9, 207–219. [https://doi.org/10.1016/0191-8141\(87\)90026-5](https://doi.org/10.1016/0191-8141(87)90026-5)
- Jolly, B. A., Lonergan, L., & Whittaker, A. C. (2016). Growth history of fault-related folds and interaction with seabed channels in the toe-thrust region of the deep-water Niger Delta. *Marine and Petroleum Geology*, 70, 58–76. <https://doi.org/10.1016/j.marpetgeo.2015.11.003>
- Jolly, B. A., Whittaker, A. C., & Lonergan, L. (2017). Quantifying the geomorphic response of modern submarine channels to actively growing folds and thrusts, deep-water Niger Delta. *Geological Society of America Bulletin*, 129, 1123–1139.

- Kergaravat, C., Ribes, C., Legeay, E., Callot, J.-P., Kavak, K. S., & Ringenbach, J.-C. (2016). Minibasins and salt canopy in foreland fold-and-thrust belts: The central Sivas Basin, Turkey. *Tectonics*, 35, 1342–1366. <https://doi.org/10.1002/2016TC004186>
- King, R. C., & Morley, C. K. (2017). Wedge geometry and detachment strength in deepwater fold-thrust belts. *Earth-Science Reviews*, 165, 268–279. <https://doi.org/10.1016/j.earscirev.2016.12.012>
- Kopriva, B. T., & Kim, W. (2015). Coevolution of minibasin subsidence and sedimentation: Experiments. *Journal of Sedimentary Research*, 85, 254–264. <https://doi.org/10.2110/jsr.2015.24>
- Krueger, S. W., & Grant, N. T. (2011). The growth history of toe thrusts of the Niger Delta and the role of pore pressure. In K. McClay, J. Shaw, & J. Suppe (Eds.), *Thrust fault-related folding* (Vol. 94, pp. 357–390). American Association of Petroleum Geologists Memoir.
- Latta, D. K., & Anastasio, D. J. (2007). Multiple scales of mechanical stratification and décollement fold kinematics, Sierra Madre oriental foreland, northeast Mexico. *Journal of Structural Geology*, 29, 1241–1255. <https://doi.org/10.1016/j.jsg.2007.03.012>
- Madof, A. S., Christie-Blick, N., & Anders, M. H. (2009). Stratigraphic controls on a salt-withdrawal intraslope minibasin, north-central Green Canyon, Gulf of Mexico: Implications for misinterpreting sea level change. *American Association of Petroleum Geologists Bulletin*, 93, 535–561. <https://doi.org/10.1306/12220808082>
- Mahanjane, E. S., & Franke, D. (2014). The Rovuma Delta deep-water fold-and-thrust belt, offshore Mozambique. *Tectonophysics*, 614, 91–99. <https://doi.org/10.1016/j.tecto.2013.12.017>
- Maloney, D., Davies, R., Imber, J., Higgins, S., & King, S. (2010). New insights into deformation mechanisms in the gravitationally driven Niger Delta deep-water fold and thrust belt. *American Association of Petroleum Geologists Bulletin*, 94, 1401–1424. <https://doi.org/10.1306/01051009080>
- Mayall, M., Lonergan, L., Bowman, A., James, S., Mills, K., Primmer, T., et al. (2010). The response of turbidite slope channels to growth-induced seabed topography. *American Association of Petroleum Geologists Bulletin*, 94, 1011–1030. <https://doi.org/10.1306/01051009117>
- Mitra, S. (1990). Fault-propagation folds: Geometry, kinematic evolution, and hydrocarbon traps. *American Association of Petroleum Geologists Bulletin*, 74, 921–945.
- Morgan, J. K. (2015). Effects of cohesion on the structural and mechanical evolution of fold and thrust belts and contractional wedges: Discrete element simulations. *Journal of Geophysical Research: Solid Earth*, 120, 3870–3896. <https://doi.org/10.1002/2014JB011455>
- Morley, C. (2009). Geometry of an oblique thrust fault zone in a deepwater fold belt from 3D seismic data. *Journal of Structural Geology*, 31, 1540–1555. <https://doi.org/10.1016/j.jsg.2009.08.015>
- Morley, C. K. (2003). Mobile shale related deformation in large deltas developed on passive and active margins. *Geological Society, London, Special Publications*, 216, 335–357. <https://doi.org/10.1144/gsl.sp.2003.216.01.22>
- Morley, C. K. (2007). Development of crestral normal faults associated with deepwater fold growth. *Journal of Structural Geology*, 29, 1148–1163. <https://doi.org/10.1016/j.jsg.2007.03.016>
- Morley, C. K., Crevello, P., & Ahmad, Z. H. (1998). Shale tectonics and deformation associated with active diapirism: The Jerudong Anticline, Brunei Darussalam. *Journal of the Geological Society*, 155, 475–490. <https://doi.org/10.1144/gsjgs.155.3.0475>
- Morley, C. K., & Guerin, G. (1996). Comparison of gravity-driven deformation styles and behavior associated with mobile shales and salt. *Tectonics*, 15, 1154–1170. <https://doi.org/10.1029/96TC01416>
- Morley, C. K., King, R., Hillis, R., Tingay, M., & Backe, G. (2011). Deepwater fold and thrust belt classification, tectonics, structure and hydrocarbon prospectivity: A review. *Earth-Science Reviews*, 104, 41–91. <https://doi.org/10.1016/j.earscirev.2010.09.010>
- Morley, C. K., & Leong, L. C. (2008). Evolution of deep-water synkinematic sedimentation in a piggyback basin, determined from three-dimensional seismic reflection data. *Geosphere*, 4, 939–962. <https://doi.org/10.1130/ges00148.1>
- Morley, C. K., & Naghadeh, D. H. (2018). Tectonic compaction shortening in Toe region of isolated listric normal fault, North Taranaki Basin, New Zealand. *Basin Research*, 30, 424–436. <https://doi.org/10.1111/bre.12227>
- Morley, C. K., von Hagke, C., Hansberry, R., Collins, A., Kanitpanyacharoen, W., & King, R. (2018). Review of major shale-dominated detachment and thrust characteristics in the diagenetic zone: Part II, rock mechanics and microscopic scale. *Earth-Science Reviews*, 176, 19–50. <https://doi.org/10.1016/j.earscirev.2017.09.015>
- Morley, C. K., von Hagke, C., Hansberry, R. L., Collins, A. S., Kanitpanyacharoen, W., & King, R. (2017). Review of major shale-dominated detachment and thrust characteristics in the diagenetic zone: Part I, meso- and macro-scopic scale. *Earth-Science Reviews*, 173, 168–228. <https://doi.org/10.1016/j.earscirev.2017.07.019>
- Moscaredelli, L., & Wood, L. (2008). New classification system for mass transport complexes in offshore Trinidad. *Basin Research*, 20, 73–98. <https://doi.org/10.1111/j.1365-2117.2007.00340.x>
- Mueller, K., & Talling, P. (1997). Geomorphic evidence for tear faults accommodating lateral propagation of an active fault-bend fold, Wheeler Ridge, California. *Journal of Structural Geology*, 19, 397–411. [https://doi.org/10.1016/s0191-8141\(96\)00089-2](https://doi.org/10.1016/s0191-8141(96)00089-2)
- Noack, T. (1995). Thrust development in the eastern Jura Mountains related to preexisting extensional structures. *Tectonophysics*, 252, 419–431.
- Nyantakyi, E. K., Li, T., Hu, W., Borkloe, J. K., Li, S., & Cheng, M. H. (2015). Structural and stratigraphic characteristics on distal parts of the outer fold and thrust belt of southern Niger Delta, Nigeria. *Arabian Journal of Geosciences*, 8, 6677–6695. <https://doi.org/10.1007/s12517-014-1727-x>
- Olayiwola, M. A., Bamford, M. K., & Durugbo, E. U. (2017). Graphic correlation: A powerful tool for biostratigraphic correlation of petroleum exploration and production in the Cenozoic deep offshore Niger Delta, Nigeria. *Journal of African Earth Sciences*, 131, 156–165. <https://doi.org/10.1016/j.jafrearsci.2017.03.028>
- Oluboyo, A. P., Gawthorpe, R. L., Bakke, K., & Hadler-Jacobsen, F. (2014). Salt tectonic controls on deep-water turbidite depositional systems: Miocene, southwestern Lower Congo Basin, offshore Angola. *Basin Research*, 26, 597–620. <https://doi.org/10.1111/bre.12051>
- Pizzi, M., Lonergan, L., Whittaker, A. C., & Mayall, M. (2020). Growth of a thrust fault array in space and time: An example from the deep-water Niger Delta. *Journal of Structural Geology*, 137, 104088. <https://doi.org/10.1016/j.jsg.2020.104088>
- Plesch, A., Shaw, J. H., & Kronman, D. (2007). Mechanics of low-relief detachment folding in the Bajiaochang field, Sichuan Basin, China. *American Association of Petroleum Geologists Bulletin*, 91, 1559–1575. <https://doi.org/10.1306/06200706072>
- Poblet, J., McClay, K., Storti, F., & Muñoz, J. A. (1997). Geometries of syntectonic sediments associated with single-layer detachment folds. *Journal of Structural Geology*, 19, 369–381. [https://doi.org/10.1016/s0191-8141\(96\)00113-7](https://doi.org/10.1016/s0191-8141(96)00113-7)
- Rouby, D., Nalpas, T., Jermannaud, P., Robin, C., Guillocheau, F., & Raillard, S. (2011). Gravity driven deformation controlled by the migration of the delta front: The Plio-Pleistocene of the Eastern Niger Delta. *Tectonophysics*, 513(1), 54–67. <https://doi.org/10.1016/j.tecto.2011.09.026>
- Rowan, M. G., Peel, F. J., & Vendeville, B. C. (2004). Gravity-driven fold belts on passive margins. In K. R. McClay (Ed.), *Thrust tectonics and hydrocarbon systems* (Vol. 82, pp. 157–182). American Association of Petroleum Geologists Memoir.



- Ruh, J. B., Vergés, J., & Burg, J.-P. (2018). Shale-related minibasins atop a massive olistostrome in an active accretionary wedge setting: Two-dimensional numerical modeling applied to the Iranian Makran. *Geology*, *46*, 791–794. <https://doi.org/10.1130/g40316.1>
- Scarselli, N., McClay, K., & Elders, C. (2016). Seismic geomorphology of Cretaceous megaslides offshore Namibia (Orange Basin): Insights into segmentation and degradation of gravity-driven linked systems. *Marine and Petroleum Geology*, *75*, 151–180. <https://doi.org/10.1016/j.marpetgeo.2016.03.012>
- Schleder, Z., Tamas, D. M., Krezsek, C., Arnberger, K., & Tulucan, A. (2019). Salt tectonics in the Bend Zone segment of the Carpathian fold and thrust belt, Romania. *International Journal of Earth Sciences(Geologische Rundschau)*, *108*, 1595–1614. <https://doi.org/10.1007/s00531-019-01721-x>
- Soto, J. I., Fernández-Ibáñez, F., Talukder, A. R., & Martínez-García, P. (2010). Miocene shale tectonics in the northern Alboran Sea (Western Mediterranean) (Vol. 93, pp. 119–144). American Association of Petroleum Geologists Memoir.
- Sun, Y., & Liu, L. (2018). Structural evolution of thrust-related folds and associated fault systems in the eastern portion of the deep-water Niger Delta. *Marine and Petroleum Geology*, *92*, 285–307. <https://doi.org/10.1016/j.marpetgeo.2017.12.012>
- Suppe, J. (1983). Geometry and kinematics of fault-bend folding. *American Journal of Science*, *283*, 684–721. <https://doi.org/10.2475/ajs.283.7.684>
- Suppe, J., Chou, G. T., & Hook, S. C. (1992). Rates of folding and faulting determined from growth strata. In K. R. McClay (Ed.), *Thrust tectonics* (pp. 105–121). London: Chapman and Hall. [https://doi.org/10.1007/978-94-011-3066-0\\_9](https://doi.org/10.1007/978-94-011-3066-0_9)
- Sylvester, Z., Cantelli, A., & Pirmez, C. (2015). Stratigraphic evolution of intraslope minibasins: Insights from surface-based model. *American Association of Petroleum Geologists Bulletin*, *99*, 1099–1129. <https://doi.org/10.1306/01081514082>
- Thyberg, B., Jahren, J., Winje, T., Bjørlykke, K., Faleide, J. I., & Marcussen, Ø. (2010). Quartz cementation in late cretaceous mudstones, northern North Sea: Changes in rock properties due to dissolution of smectite and precipitation of micro-quartz crystals. *Marine and Petroleum Geology*, *27*, 1752–1764. <https://doi.org/10.1016/j.marpetgeo.2009.07.005>
- Totake, Y., Butler, R. W. H., Bond, C. E., & Aziz, A. (2018). Analyzing structural variations along strike in a deep-water thrust belt. *Journal of Structural Geology*, *108*, 213–229. <https://doi.org/10.1016/j.jsg.2017.06.007>
- Uchupi, E. (1989). The tectonic style of the Atlantic Mesozoic rift system. *Journal of African Earth Sciences (and the Middle East)*, *8*, 143–164. [https://doi.org/10.1016/s0899-5362\(89\)80021-1](https://doi.org/10.1016/s0899-5362(89)80021-1)
- Van Rensbergen, P., & Morley, C. K. (2003). Re-evaluation of mobile shale occurrences on seismic sections of the Champion and Baram deltas, offshore Brunei. *Geological Society, London, Special Publications*, *216*, 395–409. <https://doi.org/10.1144/gsl.sp.2003.216.01.26>
- Wiener, R. W., Mann, M. G., Angelich, M. T., Molyneux, J. B., Dupuis, M., Imbert, P., et al. (2010). Mobile shale in the Niger Delta: Characteristics, structure, and evolution. *American Association of Petroleum Geologists Memoir*, *93*, 145–161.
- Wu, J. E., McClay, K., & Frankowicz, E. (2015). Niger Delta gravity-driven deformation above the relict chain and Charcot oceanic fracture zones, Gulf of Guinea: Insights from analogue models. *Marine and Petroleum Geology*, *65*, 43–62. <https://doi.org/10.1016/j.marpetgeo.2015.03.008>
- Wu, S., & Bally, A. W. (2000). Slope tectonics-comparisons and contrasts of structural styles of salt and shale tectonics of the northern Gulf of Mexico with shale tectonics of Offshore Nigeria in Gulf of Guinea. In W. Mohriak, & M. Talwani (Eds.), *Atlantic rifts and continental margins* (pp. 151–172). American Geophysical Union. <https://doi.org/10.1029/gm115p0151>
- Yang, X., Peel, F. J., McNeill, L. C., & Sanderson, D. J. (2020). Comparison of fold-thrust belts driven by plate convergence and gravitational failure. *Earth-Science Reviews*, 103–136.
- Zhang, J.-J., Wu, S.-H., Fan, T.-E., Fan, H.-J., Jiang, L., Chen, C., et al. (2016). Research on the architecture of submarine-fan lobes in the Niger Delta Basin, offshore West Africa. *Journal of Palaeogeography*, *5*, 185–204. <https://doi.org/10.1016/j.jop.2016.05.005>
- Zhang, J., Wu, S., Hu, G., Fan, T.-E., Yu, B., Lin, P., & Jiang, S. (2018). Sea-level control on the submarine fan architecture in a deepwater sequence of the Niger Delta Basin. *Marine and Petroleum Geology*, *94*, 179–197. <https://doi.org/10.1016/j.marpetgeo.2018.04.002>